PHYSICAL REVIEW
LETTERS

VOLUME 7 AUGUST 15, 1961 NUMBER 4

PLASMA PRODUCTION BY TRAVELING RESONANT PERTURBATIONS

William I. Linlor
Hughes Research Laboratories, Malibu, California
(Received June 16, 1961)

A major problem in fusion research is the production of plasma within a confining magnetic configuration. Attempts to ionize a gas initially present and to heat the ensuing plasma (as in the stellarator machine) have been beset by difficulties,[1] some of which have been explained theoretically.[2,3] Alternatively, attempts to inject energetic ions and electrons into mirror machines have been limited to low plasma densities when adiabatic conditions prevail, in agreement with theoretical analysis.[4-6]

Nonadiabatic injection methods have been investigated, such as change in charge-state[7] and entropy trapping.[8] Resonance trapping, for which the magnetic moment of a charged particle is increased by periodic interaction with magnetic field perturbations, has recently been proposed and tested.[9-12]

In this note, we propose a new method of plasma production which involves traveling resonant perturbations in an axially symmetric system. Axial symmetry is important, as otherwise loss of plasma would occur by drift motion across lines of magnetic flux. In order to avoid particle loss along paths that are mirror images of those which produced trapping initially, a nonreciprocal effect must be present. This is provided by the use of traveling perturbations, which can be achieved by well-known techniques of spatial current distribution and polyphase excitation.

Consider a modified mirror machine having a spatially periodic magnetic field on the axis of the form

$$B = B_z + B_p \cos 2\pi \left(\int \frac{dz}{\lambda(z)} - \nu_{rf} t \right), \qquad (1)$$

where B_z is the main magnetic field and varies slowly with time, the second term is a perturbing magnetic field having coordinate and time dependence as indicated, z is axial distance, λ is a wavelength and is a function of z, ν_{rf} is radio frequency, and t is time. The cyclotron frequency ν_c of a charged particle is given by

$$\nu_c = Be/2\pi m, \qquad (2)$$

where e is the electric charge in emu, m is the mass in grams, and B is in gauss. The ratio ν_{rf}/ν_c is assumed to be essentially constant and much less than unity, typically of the order of 0.01; the same is true for the ratio B_p/B_z.

The magnetic field specified by (1) is shown schematically in Fig. 1 at an arbitrary instant of time; the perturbation pattern moves from left to right at a velocity v_{rf} measured in the laboratory frame. The wavelength λ is related to the z component v_z of the velocity of the particle in the laboratory frame by the relation

$$\lambda(\nu_c + \nu_{rf}) = v_z. \qquad (3)$$

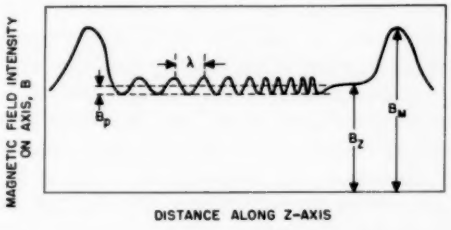

FIG. 1. Spatial variation of magnetic field intensity along axis.

It should be noted that as v_z decreases, the value of λ decreases correspondingly. The decrease in v_z is produced by conversion of velocity parallel to magnetic lines into perpendicular velocity. Transfer of kinetic energy between the particle and the traveling magnetic perturbation averages to zero because the particle is not in synchronism with the wave. During a given interaction cycle, only the "perpendicular" energy of the particle is slightly altered, but this does not affect the z component of the velocity of the particle.

Because of the large difference in ion and electron masses, simultaneous injection and trapping of a variety of positive and negative charges can be achieved in the same structure, provided that the appropriate resonance conditions for each species are satisfied.

To describe the trapping mechanism for a given particle, let us consider an off-axis particle having an initial magnetic moment μ_1 which enters at the left side of the magnetic field depicted in Fig. 1. In traversing the perturbations, the particle encounters radial components of magnetic flux. As in the system of Sinel'nikov et al.,[9] azimuthal impulses are produced by the interaction of the longitudinal component of velocity with the successive regions of radial flux. These impulses, being in resonance with the cyclotron azimuthal motion by virtue of (3), cause the magnetic moment of the particle to increase to the value μ_2 while it passes from left to right, provided that the particle enters at the appropriate phase with respect to the rf perturbation. Upon reaching the right side of the system, the particle is reflected by the mirror field B_M.

For particle motion in the right-to-left direction, the resonance condition is far from satisfied in this system, regardless of the phase of the azimuthal motion. Hence, the conversion of magnetic moment from an initial value to a larger final value is a "unidirectional" process for the system described.

Subsequent traversals of the system by the now-trapped particle will cause the magnetic moment to fluctuate,[11,12] and eventually to decrease to a sufficiently low value that the particle is no longer contained by the mirrors, in accordance with Liouville's theorem, unless time-dependent changes occur in the system. Such a change can be obtained by the adiabatic increase of B_z with time, which permits filling phase space with injected and trapped particles.

Evidently, the magnitude of the fluctuations of the magnetic moment of the trapped particles depends sensitively on the resonance conditions; it is highly desirable that at least a hundred cyclotron periods be required for conversion of the initial longitudinal velocity into perpendicular. These can be achieved by multiple passes within the same structure, employing superposed sharply resonant systems.

Interactions of the trapped particles with one another and with neutral particles, such as dissociation of molecular ions by collisions, scattering, etc., can produce sufficiently large changes in the resonance conditions that periodic decreases of B_z can be permitted without thereby producing loss of trapped particles. In such a system a practical Liouville limit in density is expected to be much greater than 10^{15} particles per cm^3, which is a density of interest in fusion power production.

The question may arise whether the traveling magnetic field would penetrate into the plasma when the latter has an appreciable conductivity. Skin depth has meaning only for conductors having fixed boundaries. For plasmas which undergo adiabatic magnetic field compression, there is no shielding of the interior because the guiding centers of all of the particles loop constant flux ϕ (Busch's theorem). Inasmuch as $d\phi/dt = 0$ for any selected element of plasma, no induced currents flow. In effect, during an adiabatic increase in the current in the external coils, the magnetic field within the plasma is compressed as if the plasma had infinite skin depth.

A detailed analysis and description of the proposed system will be given in a later publication. A remark concerning phase stability of particles near resonance seems appropriate here. In Fig. 2 we see that a reference particle having a phase angle α and exact resonance will have successive phase points labeled r. Other particles starting at r and having velocities larger or smaller than that of the reference particle will move to phase points l or s, respectively. However, a particle at l experiences a greater retardation than the

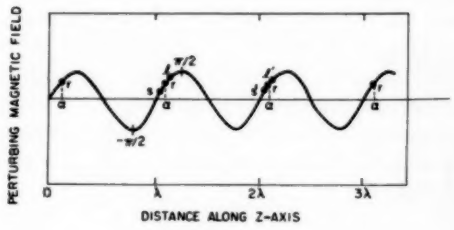

FIG. 2. Phase stability relations.

particle at r; similarly a particle at s experiences a lesser retardation than the particle at r. Thus on successive cycles the points l and s move to l' and s', and thus closer to r, giving phase stability. Obviously the argument is valid for $-\pi/2 < \alpha < \pi/2$.

It should also be remarked that the proposed system described thus far has the objective of producing a "starting plasma" which subsequently can serve as a dissociation agent for energetic injected molecular ions. Once the starting plasma has been produced regardless of the complexity and cost, subsequent continuous feeding of fusible material seems to be relatively simple.

---

[1]Proceedings of the Second International Conference on the Peaceful Uses of Atomic Energy (United Nations, Geneva, 1958), Vols. 31 and 32.

[2]S. Glasstone and R. H. Lovberg, Controlled Thermonuclear Reactions (D. Van Nostrand Company, Inc., Princeton, New Jersey, 1960), Chap. 13.

[3]W. I. Linlor, Bull. Am. Phys. Soc. 6, 193 (1961).

[4]R. F. Post, Lawrence Radiation Laboratory Report UCRL-4231, 1954 (unpublished).

[5]W. I. Linlor, Lawrence Radiation Laboratory Report UCRL-4570, 1955 (unpublished).

[6]Reference 2, p. 353.

[7]C. F. Barnett, P. R. Bell, J. S. Luce, E. D. Shipley, and A. Simon, Proceedings of the Second International Conference on the Peaceful Uses of Atomic Energy (United Nations, Geneva, 1958), Vol. 31, p. 298.

[8]J. L. Tuck, Phys. Rev. Letters 3, 313 (1959).

[9]K. D. Sinel'nikov, B. N. Rutkevich, and V. D. Fedorchenko, J. Tech. Phys. (U. S. S. R.) 30, 249 (1960) [translation: Soviet Phys.–Tech. Phys. 5, 229 (1960)].

[10]R. C. Wingerson, Phys. Rev. Letters 6, 446 (1961).

[11]H. J. Karr, E. A. Knapp, J. A. Phillips, E. J. Stovall, and J. L. Tuck, Bull. Am. Phys. Soc. 6, 379 (1961).

[12]E. W. Laing and A. E. Robson, J. Nuclear Energy C3, 146 (1961).

GENERATION OF OPTICAL HARMONICS*

P. A. Franken, A. E. Hill, C. W. Peters, and G. Weinreich
The Harrison M. Randall Laboratory of Physics, The University of Michigan, Ann Arbor, Michigan
(Received July 21, 1961)

The development of pulsed ruby optical masers[1,2] has made possible the production of monochromatic (6943 A) light beams which, when focussed, exhibit electric fields of the order of 10^5 volts/cm. The possibility of exploiting this extraordinary intensity for the production of optical harmonics from suitable nonlinear materials is most appealing. In this Letter we present a brief discussion of the requisite analysis and a description of experiments in which we have observed the second harmonic (at ~3472 A) produced upon projection of an intense beam of 6943A light through crystalline quartz.

A suitable material for the production of optical harmonics must have a nonlinear dielectric coefficient and be transparent to both the fundamental optical frequency and the desired overtones. Since all dielectrics are nonlinear in high enough fields, this suggests the feasibility of utilizing materials such as quartz and glass. The dependence of polarization of a dielectric upon electric field E may be expressed schematically by

$$P=\chi E\left(1+\frac{E}{E_1}+\frac{E^2}{E_2{}^2}+\cdots\right), \tag{1}$$

where E_1, E_2 ... are of the order of magnitude of atomic electric fields (~10^8 esu). If E is sinusoidal in time, the presence in Eq. (1) of terms of quadratic or higher degree will result in P containing harmonics of the fundamental frequency. Direct-current polarizations should accompany the even harmonics.

Let $\vec{p}$ be that part of $\vec{P}$ which is quadratic in $\vec{E}$; that is, $\vec{p}$ is a linear function of the components of the symmetric tensor $\vec{E}\vec{E}$. The eighteen coefficients which occur in this function are subject to restrictions due to the point symmetry of the medium. These restrictions are, in fact, identical with those governing the piezoelectric coefficients. In particular, $\vec{p}$ necessarily vanishes in a material such as glass which is isotropic or contains a center of inversion. For crystalline quartz, however, there are two independent coefficients α and β in terms of which

$$\begin{aligned} p_x &= \alpha(E_x{}^2-E_y{}^2)+\beta E_y E_z, \\ p_y &= -\beta E_x E_z-2\alpha E_x E_y, \\ p_z &= 0 \end{aligned} \tag{2}$$

Table I. The square of the total p perpendicular to the direction of propagation of light through crystalline quartz.

Direction of incident beam	The square of the total p perpendicular to direction of propagation
x ($E_x=0$)	$p_y{}^2+p_z{}^2=0$
y ($E_y=0$)	$p_z{}^2+p_x{}^2=\alpha^2E_x{}^4$
z ($E_z=0$)	$p_x{}^2+p_y{}^2=\alpha^2(E_x{}^2+E_y{}^2)^2$

(z is the threefold, or optic, axis; x a twofold axis). If a light beam traverses quartz in one of the three principal directions, Eqs. (2) predict the results summarized in Table I. The second-harmonic light should be absent in the first case, dependent upon incident polarization in the second case, and independent of this polarization in the third.

If an intense beam of monochromatic light is focussed into a region of volume V, there should occur an intensity I of second harmonic given (in Gaussian units) by

$$I\sim(\omega^4/c^3)(pv)^2(V/v), \tag{3}$$

where ω is the angular frequency of the second harmonic, c the velocity of light, and v an effective "volume of coherence"; that is, the size of a region within the sample in which there is phase coherence of the p excitation. (This volume may in practice be much smaller than V.) An estimate of v is governed by several considerations. For example, it is probably of no greater extent in the propagation direction than $\sim[n_2\times(n_2-n_1)^{-1}]\lambda_2$, where n_1 and n_2 are the indices of refraction for the fundamental and second harmonic frequencies, respectively, and λ_2 is the wavelength of the second harmonic. The lateral extent of this volume is determined in large part by the coherence characteristics of the optical maser. The situation for a maser of the gas discharge[3] type is clearly more favorable in this respect than that for the ruby device.[1,2] For a coherence volume of 10^{-11} cm^3, which we think may be realistic in our case, Eq. (1) indicates

FIG. 1. A direct reproduction of the first plate in which there was an indication of second harmonic. The wavelength scale is in units of 100 A. The arrow at 3472 A indicates the small but dense image produced by the second harmonic. The image of the primary beam at 6943 A is very large due to halation.

that second harmonic intensities as high as a fraction of a percent of the fundamental could be achieved.

In the experiments we have used a commercially available ruby optical maser[4] which produces approximately 3 joules of 6943A light in a one-millisecond pulse. This light is passed through a red filter for the elimination of the xenon flash background and is then brought to a focus inside a crystalline quartz sample. The emergent beam is analyzed by a quartz prism spectrometer equipped with red insensitive Eastman Type 103 spectrographic plates. A reproduction of the first plate in which there was an unambiguous indication of second harmonic (3472 A) is shown in Fig. 1. This plate was exposed to only one "shot" from the optical maser. We believe the following two facts, among others, rule out the possibility of artifact:

(1) The light at 3472 A disappears when the quartz is removed or is replaced by glass.

(2) The light at 3472 A exhibits the expected dependence on polarization and orientation summarized in Table I.

Considerations of the photographic image density and the efficiency of the optical system lead us to believe that the order of 10^{11} second harmonic photons were generated within the quartz sample per pulse.

The production of a second harmonic should be observable in isotropic materials such as glass if a strong bias field were applied to the sample. This bias could be oscillatory, thus producing sidebands on the fundamental frequency and the harmonics.

We would like to thank the staff of Trion Instruments, Inc., for their valuable and sustained cooperation in this work.

---

*This work was supported in part by the U. S. Atomic Energy Commission.

[1]T. H. Maiman, Nature 187, 493 (1960).

[2]R. J. Collins et al., Phys. Rev. Letters 5, 303 (1960).

[3]A. Javan, W. R. Bennet, and D. R. Herriott, Phys. Rev. Letters 6, 106 (1961). Even though the intensity of the gas device is very low compared with ruby masers, the gain in coherence volume and the potential improvement of focussing suggest that the gas maser may be comparable or even superior as a source for optical harmonics.

[4]Trion Instruments, Inc., Model No. TO-3000.

DIRECT DETERMINATION OF X-RAY REFLECTION PHASE RELATIONSHIPS THROUGH SIMULTANEOUS REFLECTION*

M. Hart and A. R. Lang

H. H. Wills Physics Laboratory, University of Bristol, Bristol, England

(Received July 18, 1961)

This Letter reports a successful direct experimental determination of x-ray reflection phase relationships through coherent dynamical interactions in simultaneous x-ray reflection. When a crystal is so oriented with respect to the incident beam that both reflections h $(=hkl)$ and h' $(=h'k'l')$ are excited, the region in reciprocal space concerned is in the vicinity of the point of intersection of the three spheres Σ_0, Σ_h, and $\Sigma_{h'}$ centered, respectively, on reciprocal lattice points O, h, and h', the radii of the spheres being $\kappa = nK$ where n is the crystal refractive index and K the free-space wave number for the radiation used. In this region the dispersion surface is made up of three sheets, and in the crystal there are nine wave vectors $\vec{k}_g^{(i)}$ $(g = O, h, h'; i = 1, 2, 3)$. (For diffraction at low angles, polarization effects may be neglected; otherwise one would have to consider six sheets.) Clearly the situation is very complicated when all the diffracted waves are comparable in amplitude. However, we have achieved our result in a straightforward way by three steps.

(1) High-resolution x-ray diffraction topographs[1,2] are used to provide adequate definition of angular and spatial relations.

(2) A valuable simplification is gained by restricting attention to an investigation of the modification of the dispersion surface of the h reflection as one proceeds along the line of intersection of Σ_0 and Σ_h and approaches the intersection with $\Sigma_{h'}$.

(3) For studying small modifications of the dispersion surface we make use of the phenomenon of Pendellösung interference. It has been shown[3,4] that in x-ray projection topographs[2] of wedge-shaped crystals in the Laue case the Pendellösung fringe pattern is determined by the minimum diameter of the dispersion surface hyperbolae, which is proportional to the structure amplitude $|F_h|$. The fringe spacing, for a given wedge angle, is inversely proportional to this diameter. In the present investigation, displacements of Pendellösung fringes on the topograph provide the measure of modifications of the dispersion surface.

The geometry of the experiments is explained in the stereographic projection, Fig. 1. The

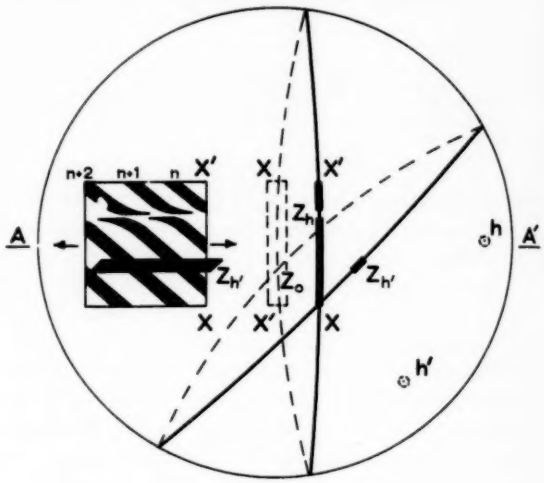

FIG. 1. Diffraction geometry for simultaneous reflection.

crystal (not shown) is at the center of the sphere. Diffracted beams lie in the hemisphere above the paper, whereas the incident beam lies in the hemisphere below the paper. Continuous and interrupted lines are used, respectively, on the hemispheres above and below the paper. The line AA' represents the horizontal and the crystal is illuminated by a narrow vertical ribbon of x rays. The angular range of the incident-ray bundle is represented by the interrupted rectangle, much exaggerated in the drawing. The x-ray source is effectively a point and the vertical range of incident rays is determined by the height of crystal illuminated. There is thus a one-to-one correspondence between position on the crystal and the vertical angle of the ray incident upon it. The plane normals h and h' are shown, together with the cones generated by all rays making the appropriate Bragg angle with these planes for the radiation used (Ag $K\alpha_1$). The plane normal h lies horizontal and the whole of the incident beam straddles the h cone. A diffracted beam the full height of the crystal is thus obtained, incident rays X and X' giving rise to diffracted rays X and X', respectively. Next, the crystal

is rotated about plane normal h to bring the h' cone into the incident beam, but in this case the incident beam cuts only a small part of the cone. The incident ray common to both the h cone and h' cone is at Z_0, the small bundle of the h' diffracted beam is at $Z_{h'}$, and in the extended h diffracted beam we find an Aufhellung[5] in the direction Z_h corresponding to the incident ray Z_0. The crystal has the shape of a gently tapering wedge, with the thickness contours making a moderate angle with the horizontal. The projection topograph obtained by traversing the crystal back and forth appears as sketched in the left-hand part of Fig. 1. The thin end of the wedge is in the upper right and the Pendellösung fringe order is in the sequence indicated. (The diffracted beam $Z_{h'}$ may possibly pass through the diffracted beam screening slits and appear as a streak as shown.)

The electron diffraction dynamical theory of Kambe and Miyake,[6,7] modified to the x-ray case, shows that in the vicinity of $\Sigma_{h'}$ the minimum diameter of the h reflection dispersion surface hyperbolae is proportional not to $|F_h|$ but to quantities $|F_+|$ just inside $\Sigma_{h'}$, and $|F_-|$ just outside $\Sigma_{h'}$, to a good approximation. Whether $|F_+|$ is greater or less than $|F_-|$ depends upon whether $\cos\Phi_{hh'}$ is positive or negative, $\Phi_{hh'}$ being a function of the individual phase angles, α, of the reflections h, h', and $h'-h$,

$$\Phi_{hh'} = \alpha_h - \alpha_{h'} + \alpha_{h'-h}.$$

In a centrosymmetric cyrstal, $\Phi_{hh'}$ can only be zero or π; hence $\cos\Phi_{hh'}$ is then restricted to the values ± 1. Now wave vectors of rays incident between X and Z_0 (and hence diffracted between X and Z_h) lie outside $\Sigma_{h'}$, whereas those incident between X' and Z_0 lie inside $\Sigma_{h'}$. Thus, on the topograph, one expects the effective diameter of dispersion surface hyperbolae to be proportional to $|F_+|$ just above the Aufhellung, and to $|F_-|$ just below the Aufhellung. Hence if $|F_+|$ is greater than $|F_-|$ the Pendellösung fringe spacing is decreased above the Aufhellung and increased below; and vice versa. In the former case the fringe discontinuity appears as sketched. The experiment is quite a sensitive one, since at the fringe of order 5, a change of only 10% in dispersion surface diameter will shift the fringes by half a period.

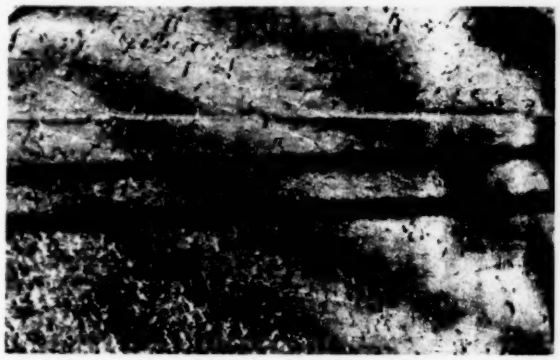

FIG. 2. Diffraction topograph showing dislocation of Pendellösung fringes at an Aufhellung.

A topograph corresponding to the sketch in Fig. 1 is shown in Fig. 2. The crystal is germanium, the reflection h is $2\bar{2}0$ and the reflection h' is $3\bar{1}\bar{1}$. The Aufhellung appears across the field and the streaks due to the h' reflection (both $K\alpha_1$ and $K\alpha_2$) appear across the lower half. Although the crystal thickness variation is not as smooth as could be desired, and numerous dislocations are scattered over the field, the form of the shift of the Pendellösung fringes clearly shows that $|F_+|$ is greater than $|F_-|$.

Since the structure is centrosymmetric, the observation shows that $\cos\Phi_{hh'}=1$, and hence $\Phi_{hh'}=\alpha_h-\alpha_{h'}+\alpha_{h'-h}=0$. This result is in agreement with that calculated for the known structure. A direct experimental determination of phase relationships is thus effected.

The authors would like to thank Professor F. C. Frank and Professor S. Takagi for advice.

---

*This research has been sponsored in part by the Wright Air Development Division, Air Research and Development Command, U. S. Air Force, through its European Office.

[1]A. R. Lang, Acta Met. 5, 358 (1957).
[2]A. R. Lang, Acta Cryst. 12, 249 (1959).
[3]N. Kato and A. R. Lang, Acta Cryst. 12, 787 (1959).
[4]N. Kato, Acta Cryst. 14, 526, 627 (1961).
[5]G. Meyer, Z. Krist. 66, 585 (1928).
[6]K. Kambe and S. Miyake, Acta Cryst. 7, 218 (1954); S. Miyake and K. Kambe, Acta Cryst. 7, 220 (1954); K. Kambe, Acta Cryst. 7, 777 (1954).
[7]K. Kambe, J. Phys. Soc. Japan 12, 13, 25 (1957).

EXPERIMENTAL TEST OF THE SPIN-WAVE THEORY OF A FERROMAGNET

A. C. Gossard, V. Jaccarino, and J. P. Remeika
Bell Telephone Laboratories, Murray Hill, New Jersey
(Received July 24, 1961)

A detailed theory of the thermodynamic properties of an idealized model of a ferromagnet, in which there exist only temperature-independent ferromagnetic nearest neighbor interactions having the form $J\sum_{i}^{nn}\vec{S}\cdot\vec{S}_i$, has been given.[1] There has hitherto been no satisfactory test of the theory, primarily because no known ferromagnetic materials satisfied the assumptions of the model. Recently, Tsubokawa[2] has discovered an insulating ferromagnet, $CrBr_3$, which closely approximates the model. Using nuclear magnetic resonance (NMR) techniques, we have made a precise measurement of the temperature dependence of the magnetization of this compound.

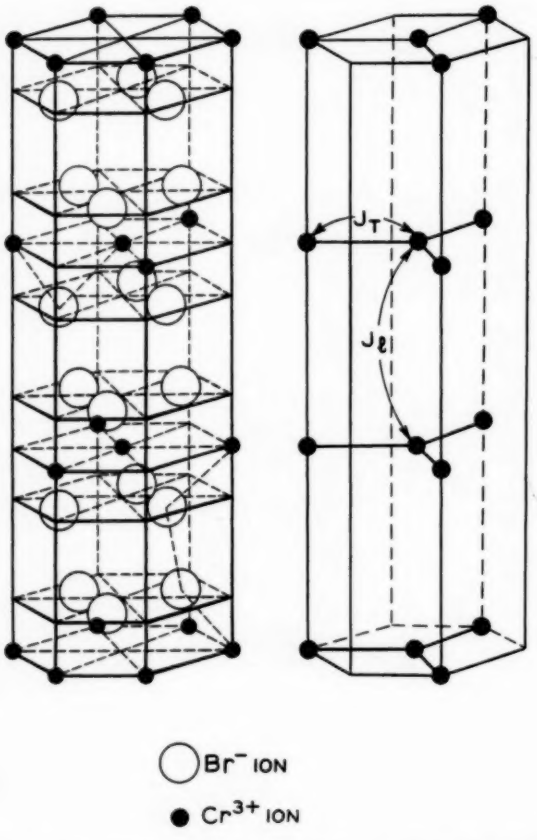

FIG. 1. Crystal structure of $CrBr_3$ (from Tsubokawa). The Br^- ions form a nearly perfect close-packed hexagonal structure. The Cr^{3+} ions occupy two-thirds filled hexagonal layers with two Br^- layers separating each Cr^{3+} layer. Each Cr^{3+} is surrounded by a nearly perfect octahedron of Br^- ions. At the right a simplified model used to calculate the spin-wave dispersion law is shown.

$CrBr_3$ has the DO_5 (BiI_3) hexagonal layer structure[3] shown in Fig. 1 and is prepared by heating powdered chromium in an atmosphere of bromine at 800°C.[2] Tsubokawa has measured several of its magnetic properties. In particular he has found a ferromagnetic Curie point $T_C = 37°K$ and a saturation magnetization of $3\mu_B$ per Cr^{3+} ion as would be expected for the $3d^3\ {}^4S$ configuration in an octahedral crystal field. For the purely ionic ^4S configuration a 375 000-oersted negative internal field at the Cr nucleus would be expected as a result of the exchange polarization of inner closed-shell s electrons by the aligned d electrons.[4] Since overlap of the Cr and Br wave functions and covalent bonding reduce the magnitude of the internal field at the Cr nucleus, we searched for the Cr^{53} NMR in the frequency region below 85 Mc/sec using a frequency-swept modified Robinson marginal oscillator.[5]

An oscilloscope tracing of the spectrum observed at 58.038 Mc/sec ($H_{hfs} = 241\,220$ oe) and 1.34°K in zero external field is shown in the upper corner of Fig. 2. Three distinct absorptions are seen, whose separations and intensities correspond to the allowed transitions for $I = \frac{3}{2}$ and a nuclear electric quadrupole interaction $h^{-1}e^2q_{zz}Q = 1.184$ Mc/sec.

The occurrence of sharp satellites indicates a uniform orientation of the internal magnetic field with respect to the axes of the electric field gradient tensor. From this, and the external field dependence of the frequency for resonance, it may be concluded that the nuclei participating in the resonance are situated in the body of the domains and not in the domain walls. Enhancement of the resonant absorption occurs from domain rotation rather than wall motion.[6] The sign of the magnetic field at the nuclei was determined to be negative with respect to the direction of magnetization from the observed decrease of the resonance frequency with increasing external field. The temperature dependence of the Cr^{53} NMR is shown in Fig. 2. The resonance was observed up to 15°K.[7]

Because of the hfs interaction $A\vec{I}\cdot\vec{S}$ between

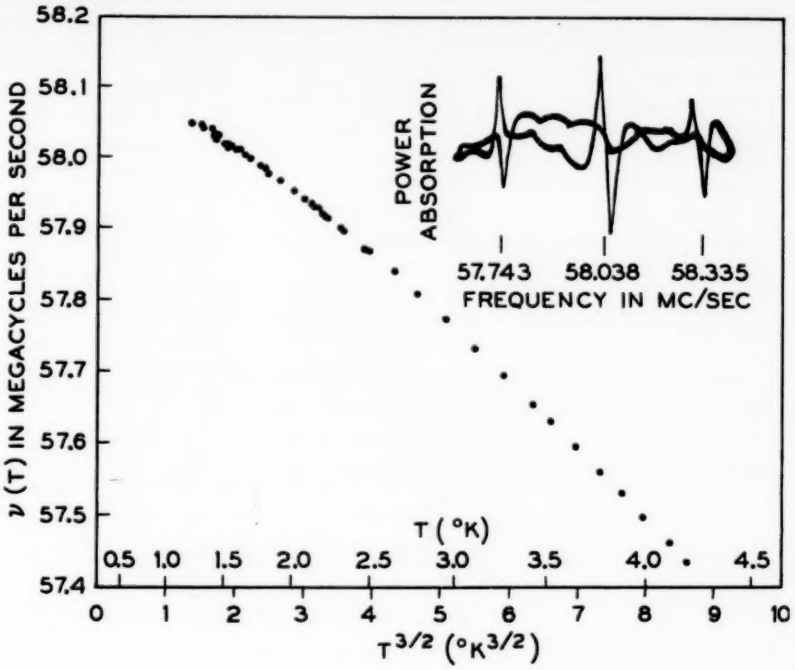

FIG. 2. Cr^{53} nuclear resonance frequency vs temperature in $CrBr_3$ in zero applied magnetic field. An oscillographic picture of the resonances at 1.34°K is shown above. Differences in the shape of the resonances on forward and return sweep are caused by passing through the lines in times comparable to nuclear relaxation times.

the ionic spin $\vec{S}$ and the nuclear spin $\vec{I}$, NMR is observable at a temperature $T<T_c$ at a frequency $\nu(T)=h^{-1}A\langle S\rangle_T$, where $\langle S\rangle_T$ is the thermal average of $\vec{S}$. Since $M(T)=Ng\beta\langle S\rangle_T$, we expect $\nu(T)$ to be proportional to $M(T)$ provided that A depends neither implicitly nor explicitly on T. The temperature dependence of hfs interactions has been investigated in other magnetic solids.[8] The results of such studies lead us to conclude that the variation of A between 0° and 4°K, in $CrBr_3$, is considerably less than the intrinsic precision of our experiment (1 part in 30 000).

The spin-wave prediction[9] for the temperature dependence of the spontaneous magnetization $M(T)$, for $T\ll T_c$ is,

$$M(T)=M(0)[1-aT^{3/2}-bT^{5/2}-cT^{7/2}-dT^{4}-eT^{9/2}-\cdots]. \quad (1)$$

The half-odd-integral terms beyond $T^{3/2}$ result from the discreteness of the lattice, while the T^4 term is the lowest spin-wave interaction term. In the case of cubic symmetry with no external field or anisotropy, the coefficients a, b, c, d, and e are functions only of J, S and the lattice geometry. In the DO_5 lattice, however, several exchange interactions are involved. Nearest neighbor spins within a layer are strongly coupled by superexchange through a single intervening ion. Exchange between spins in adjacent layers is weaker because two intervening ions in series separate the interacting spins. Calculation of the expected magnetization coefficients is thus complicated by the fact that some weak exchange is expected even for spins not directly above one another. To simplify calculation of the coefficients, we have adopted a model of the lattice shown at the right in Fig. 1. Only two exchange interactions, J_l and J_t, are considered in the spin-wave calculation. For $J_l\ll J_t$ we obtain $a=0.0130\,J_l^{-1/2}J_t^{-1}$ and $b=0.000140\,J_l^{-3/2}J_t^{-1}$. In the presence of a magnetic or anisotropy field, H, the $T^{3/2}$ coefficient in the same formalism becomes

$$(a/2.612)\textstyle\sum_n[n^{-3/2}\exp(-ng\beta H/kT)].$$

The other coefficients are modified similarly.

In Fig. 2 the results of the NMR measurements are plotted against $T^{3/2}$ for $T<0.11\,T_c$. At the lowest temperatures the effect of the anisotropy-modified $T^{3/2}$ term is seen to predominate. Using Dillon's observed value[10] of 6850 oersteds for the anisotropy field, a least-squares fit of the form

$$\nu(T)=\nu(0)\left[1-\frac{a}{2.612}\sum_n\frac{e^{-ng\beta H/kT}}{n^{3/2}}T^{3/2}-\frac{b}{1.341}\sum_n\frac{e^{-ng\beta H/kT}}{n^{5/2}}T^{5/2}\right],$$

was made. $\nu(0)$ was determined to be 58.096 Mc/sec, corresponding to a field at the nucleus of 241 460 oersteds. a was $(2.544 \pm 0.067) \times 10^{-3}\,°K^{-3/2}$, b was $(3.03 \pm 1.04) \times 10^{-5}\,°K^{-3/2}$, and the mean square square deviation of the data points from the fit was 0.0016 Mc/sec. Inclusion of $T^{7/2}$ and T^4 terms does not significantly improve the fit. From a and b we calculate that $J_t = 5.44°K$ and $J_l = 0.88°K$. The smallness of J_l relative to J_t, inferred from inspection of the superexchange "paths," is thus confirmed, and manifests itself in the magnetization curve as an unusually large $T^{3/2}$ term.

We wish to thank R. J. Blume for the circuit of the Robinson-type spectrometer, J. L. Davis for experimental assistance, E. M. Kelley for aid in growing the crystals, and Dr. L. R. Walker for theoretical counsel.

[1]F. Bloch, Z. Physik 74, 295 (1932).
[2]Ichiro Tsubokawa, J. Phys. Soc. Japan 15, 1664 (1960).
[3]Å. Braekken, Kgl. Norske Videnskab. Selskab, Forh. 5, No. 11 (1932).
[4]V. Heine, Phys. Rev. 107, 1002 (1957).
[5]F. N. H. Robinson, J. Sci. Instr. 36, 481 (1959); R. J. Blume (to be published).
[6]A. M. Portis, A. C. Gossard, R. H. Lindquist, and M. Rubinstein (to be published).
[7]R. G. Barnes and S. L. Segel have observed Br^{81} nuclear quadrupole resonance in the paramagnetic state of $CrBr_3$. R. G. Barnes and S. L. Segel, Phys. Rev. Letters 3, 462 (1959).
[8]G. B. Benedek and J. Armstrong, J. Appl. Phys. 32, 106S (1961); V. Jaccarino and L. R. Walker (to be published).
[9]Freeman J. Dyson, Phys. Rev. 102, 1230 (1956).
[10]We are indebted to J. F. Dillon for communication of this result before publication.

PHASE TRANSITION IN MERCURY TELLURIDE*

J. Blair and A. C. Smith
Department of Electrical Engineering, Massachusetts Institute of Technology, Cambridge, Massachusetts
(Received July 17, 1961)

An abrupt change in the resistivity of mercury telluride has been observed at a pressure of about 15 000 kg/cm² at room temperature. This change is ascribed to a transition between two polymorphic phases of HgTe. The resistivity changes essentially reversibly by a factor of 10^4 to 10^5 at this transition. No information about the structure of the high-pressure phase has been obtained.

Figure 1 shows the variation of the resistivity of a sample of HgTe as a function of pressure. The resistivity was measured with a four-probe method using a precision potentiometer. At 16 000 kg/cm², the resistivity increases by a factor greater than 10^4. The transition takes place very slowly and the points above 16 000 kg/cm² do not represent an equilibrium situation. The time that elapsed while the sample was in the high-pressure phase was several hours and the resistivity drifted upward consistently. As the pressure was decreased, the reverse transition occurred at 12 000 kg/cm². The resistivity decreased by a factor of 10^4, but did not quite return to its original value.

When the sample was examined, several cracks were found. These cracks presumably account for the difference in the atmospheric pressure values of the resistivity before and after the application of pressure. The sample was initially a single crystal and if the transition nucleated at a number of points, the sample would be polycrystalline after the transition. The strains arising from misorientation of the crystallites would produce the observed cracks.

The resistivity of this sample before the pressure experiment was 1.5×10^{-3} ohm cm. Meas-

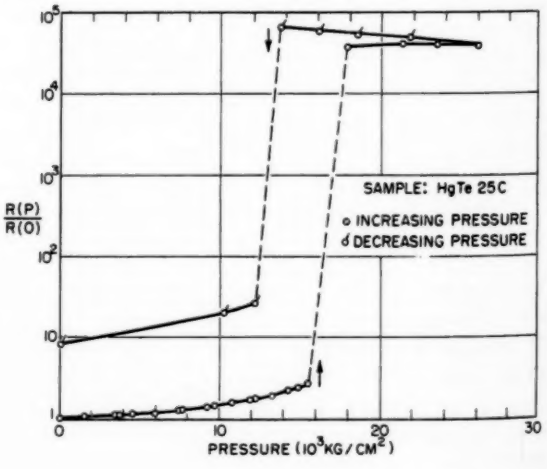

FIG. 1. Normalized resistance of HgTe vs pressure. Arrows show pressures at which transition occurred.

urements by Nelson[1] on adjacent samples from the same ingot yield an acceptor concentration of 3.7×10^{18} cm^{-3}, and an electron mobility of 2.3×10^{4} cm^2/volt sec. The change in resistivity below the transition pressure is quite reproducible and is essentially the same for samples from different ingots. A detailed explanation of this behavior is planned for a later paper.

The phase transition was observed in another sample of HgTe and an effort was made to determine the transition pressure more accurately. The limits of the transition pressure were again found to be 16 000 kg/cm^2 with increasing pressure and 12 000 kg/cm^2 with decreasing pressure.

The authors wish to express their thanks to Professor William Paul and the High Pressure Group at Harvard University for the use of the pressure equipment. We also thank Dr. R. E. Nelson for supplying the HgTe samples.

---

*This work was partially supported by the Air Force Cambridge Research Laboratories (Air Research and Development Command), U. S. Air Force.

[1]R. E. Nelson, Sc.D. thesis, Department of Electrical Engineering, Massachusetts Institute of Technology (unpublished).

NEGATIVE PION-PROTON ELASTIC SCATTERING AT 1.51, 2.01, AND 2.53 Bev/c OUTSIDE THE DIFFRACTION PEAK*

Kwan W. Lai,† Lawrence W. Jones, and Martin L. Perl
The University of Michigan, Ann Arbor, Michigan
(Received July 27, 1961)

The differential elastic scattering cross sections for negative pions on protons have been measured at incident pion momenta of 1.51, 2.01, and 2.53 Bev/c with emphasis on the angular region outside the diffraction peak. The purpose of the experiment was to examine the behavior of the large angle differential elastic cross section as a function of energy from the energy of the highest known resonance in the pion-nucleon system into the region where the total cross sections appear to be approaching an asymptotic value.[1]

The experiment was performed at the Bevatron using a luminescent chamber system to photograph the tracks of the scattered pion and the recoil proton from a liquid hydrogen target. The chamber configuration used is shown in Fig. 1, where the plane of the figure is normal to the optic axis of the image intensifier tube system. Lenses focused this image of the sodium iodide scintillators onto the first image tube cathode, and the gain of the system was sufficient to record single photoelectrons from this cathode. A coincidence between the coplanarity counters, which subtended $\Delta\Phi=\pm7.15°$ from the vertical plane, triggered the system on probable elastic events. This post-event triggering enabled the tracks to be subsequently recorded on film with a time resolution of a few microseconds. A description of the apparatus has been reported elsewhere in detail.[2] The film was double scanned, and angles for elastic scattering events were recorded with suitable corrections for distortions in the image tube system. The angles and ionization of the two tracks were used to identify an event as elastic, and subsequent correlations of the track angles with kinematics were consistent

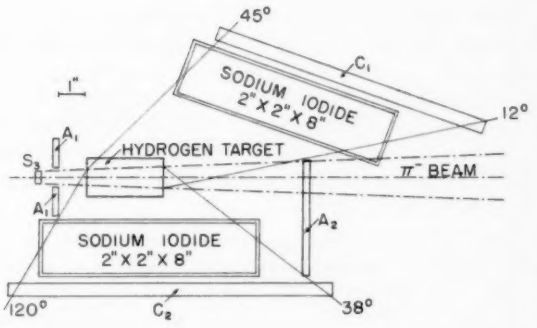

FIG. 1. Geometry of liquid hydrogen target, scintillation counters, and sodium iodide luminescent chambers. The coplanarity scintillation counters C_1 and C_2 subtended ±7.15° from the vertical plane (the plane of the drawing) for scatterings on the beam axis. Besides anticoincidence counters A_1 and A_2, two other anticoincidence counters flanked the target parallel to the plane of the figure to bias against inelastic events. S_3 is the final beam defining counter. The sodium iodide crystals were imaged by lenses onto the image tube system which was oriented perpendicularly to the plane of the figure.

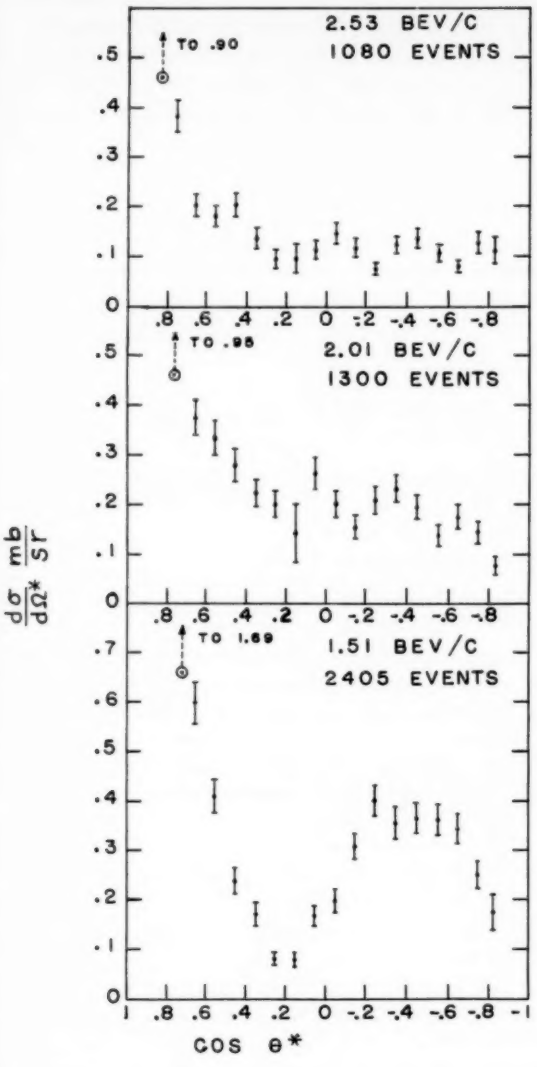

FIG. 2. Elastic differential cross section of $\pi^- + p \rightarrow \pi^- + p$ in the center-of-momentum system. θ^* is the angle of the scattered pion in that system. The values of $d\theta/d\Omega^*$ at the smallest angle measured at each energy are too large to be placed at the correct places on the graphs, but their values are indicated.

with the known angular resolution of the measurements.

2405 elastic scatterings were analyzed at 1.51 Bev/c, 1300 events at 2.01 Bev/c, and 1080 events at 2.53 Bev/c. The results are presented in Fig. 2. The differential cross sections have been corrected for multiple Coulomb scattering and nuclear interactions in sodium iodide, for geometrical and scanning biases, and for pseudo-elastic events from the target vessel (from data taken with the target empty). The absolute value of the differential cross section may be uncertain by as much as ±15% from systematic errors associated with this new technique. The data at 1.51 Bev/c are in good agreement with the bubble chamber result of Chretien et al.[3]

From the data it may be noted that the backward hump, which has a maximum height of 2.1 mb/sr at 900 Mev and 1.1 mb/sr at 1020 Mev,[4] is down to 0.4 mb/sr at 1.51 Bev/c (1.37 Bev) and is not present at 2.01 or 2.53 Bev/c. The angular distributions behind the diffraction peak at 2.01 and 2.53 Bev/c are roughly constant with angle, decreasing from 0.18 mb/sr at 2.01 Bev/c to 0.11 mb/sr at 2.53 Bev/c. Although the data at these two higher momenta can be taken to suggest some oscillatory structure behind the diffraction peak, they are not inconsistent with an isotropic distribution behind the diffraction peak.

We wish to acknowledge our appreciation to Dr. E. J. Lofgren, his associates, and the staff of the Bevatron of the Lawrence Radiation Laboratory for their hospitality and assistance throughout the preparation, execution, and analysis of this experiment.

---

*This work was supported by the Office of Naval Research.

†Submitted by Kwan W. Lai in partial fulfillment of the requirement for the degree of Doctor of Philosophy.

[1]V. S. Barashenkov, Soviet Phys.-Uspekhi 3, 689 (1961).

[2]M. L. Perl, L. W. Jones, and K. Lai, in Proceedings of the 1960 International Conference on Instrumentation for High-Energy Physics (Interscience Publishers, Inc., New York, 1961), p. 186.

[3]M. Chretien, J. Peitner, N. P. Samios, M. Schwartz, and J. Steinberger, Phys. Rev. 108, 383 (1957).

[4]C. D. Wood, T. J. Devlin, J. A. Helland, M. J. Longo, B. J. Meyer, and V. Perez-Mendez, Phys. Rev. Letters 6, 481 (1961).

TOTAL CROSS SECTIONS FOR PIONS ON PROTONS IN THE MOMENTUM RANGE 4.5 TO 10 Gev/c

G. von Dardel, R. Mermod, P. A. Piroué,* M. Vivargent, G. Weber, and K. Winter
CERN, Geneva, Switzerland
(Received July 17, 1961)

In a previous paper[1] we reported on measurements of total cross sections for p, $\bar{p}$, $K^{\pm}$, and $\pi^{\pm}$ on protons at high energy. According to a theorem given by Pomeranchuk,[2] the total cross sections for a particle and its antiparticle must become equal if they approach constant values at high energy. For pions, the conditions of this theorem are thought to be fulfilled at lower energies than for the other particles. In our previous paper, a large uncertainty on the muon contamination did not allow us to draw any significant conclusion concerning the validity of the Pomeranchuk theorem.

The present paper reports on a more accurate measurement of the $(\pi^{\pm}, p)$ total cross sections in the momentum range 4.5 to 10 Gev/c; the experimental method used eliminated the effect of muon contamination on the cross sections.

The layout of the experiment is shown in Fig. 1. A beam of secondary particles enters the experimental hall and comes to a focus at the center of a velocity-selective gas Čerenkov counter $\check{C}$, after having traversed a system of two quadrupole lenses and a bending magnet located in the target area. The beam spot at the Čerenkov counter is imaged by another doublet of quadrupole lenses, Q_3, Q_4, onto transmission counters, S_4, S_5, S_6, which are located behind a 312-cm long liquid hydrogen target. Bending magnet B_2 provides a second momentum analysis eliminating secondaries from reactions produced in the collimator walls, in the Čerenkov counter, and in the air, and also eliminating part of the decay muons. The beam incident on the hydrogen target is defined by scintillation counters, S_1, S_2, and S_3, 2, 5, and 2 cm in diameter, respectively, operated in coincidence with the Čerenkov counter, which is set to count pions, but does not discriminate against muons and electrons. After traversing the transmission counters S_4, S_5, and S_6, having diameters of 10, 15, and 20 cm, respectively, the beam is intercepted by a 1-mm long iron absorber in which strongly interacting particles and electrons are lost, whereas more than 99% of the muons are transmitted into counter S_7 (30 cm in diameter). The pions transmitted into counters S_4, S_5, and S_6 are signalled by the coincidences $(S_1S_2S_3\check{C}S_4\bar{S}_7)$, $(S_1S_2S_3\check{C}S_5\bar{S}_7)$, and $(S_1S_2S_3\check{C}S_6\bar{S}_7)$, respectively. These rates, normalized to the incident rate $(S_1S_2S_3\check{C})$, were measured for both target "full" and target "empty." Two steel plates of appropriate thickness simulated the empty target. The coincidence logics was arranged such that the time resolution in all channels was determined by threefold coincidence units of 5-nsec resolution. The accidental rates were negligibly small.

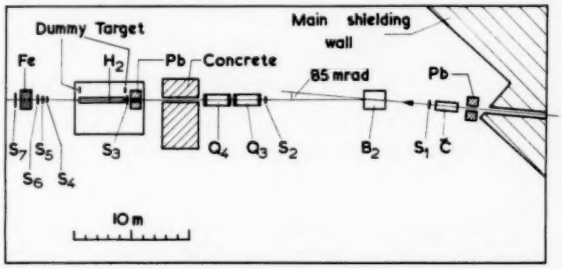

FIG. 1. Experimental layout. The first doublet of quadrupoles and the first bending magnet are in the target area (not shown). Lead collimators shown are 2.5 $\times$2.5 cm^2, S_1-S_7 scintillators, Q_{3-4} quadrupole lenses, B_2 second bending magnet.

The electron contamination in the negative beam was estimated to 0.6% at 6 Gev/c from a measurement using a threshold Čerenkov counter in a similar beam, and a calculation of the effect of radiation losses in the material in the actual beam used in the experiment. All sources of positron contamination are expected to yield a smaller fraction in the positive beam. In both beams, the contamination is decreasing with increasing energy. The correction to the cross section and to the difference $\sigma(\pi^-, p) - \sigma(\pi^+, p)$ will be less than 0.2 mb.

Earlier measurements of the transmission in hydrogen of negative pions had shown that there is no structure within 3% of the cross section for either isospin state in the momentum range 5-10 Gev/c. Therefore, it was sufficient in the present work to measure cross sections at a few momenta only (4.5, 5.75, 7.0, and 10.0 Gev/c).

Total cross sections were obtained by extrapolating to zero solid angle the cross sections measured with counters S_4, S_5, and S_6, subtending solid angles averaged over the target length of 0.469, 0.826, and 1.315 msr, respectively.

Table I. Total cross sections for negative and positive pions on protons and their difference.

Momentum (Gev/c)	$\sigma(\pi^-,p)$ (mb)	$\sigma(\pi^+,p)$ (mb)	$\sigma(\pi^-,p)-\sigma(\pi^+,p)$ (mb)
4.5	30.2 ± 0.4	27.6 ± 0.3	2.6 ± 0.5
5.75	29.1 ± 0.4	26.9 ± 0.4	2.2 ± 0.6
7.0	28.4 ± 0.4	26.1 ± 0.3	2.3 ± 0.5
10.0	27.0 ± 0.4	25.2 ± 0.4	1.8 ± 0.6

For the lowest momentum, a correction for multiple scattering of 1.3% was applied to $\sigma(S_4)$. The cross sections plotted versus solid angle form a straight line at all momenta, and consequently, linear extrapolation to zero solid angle was used to derive the total cross section. The results are given in Table I.

The errors given are statistical only, including the error in extrapolation. The absolute values of the cross sections may have an additional error of about 0.5 mb due to uncertainties in the effective target length and the calibration of the steel plates simulating the empty target. This should affect neither the difference of cross sections for negative and positive pions, nor the momentum dependence.

The results are shown in Fig. 2 together with data of other authors.[3-7] Our value for the (π^+, p) cross section at 4.5 Gev/c is lower than values given by Longo et al.[3] and Chzan et al.[7]

Unlike the situation for (p, p) total cross sections[8] which have been shown to be constant between 5 and 28 Gev/c, a monotonic decrease is observed for both the (π^+, p) and (π^-, p) cross section with increasing energy. Hence, the condition for Pomeranchuk's theorem[2] that total cross sections tend asymptotically to constant values is not satisfied for the π-nucleon system up to 10 Gev/c.

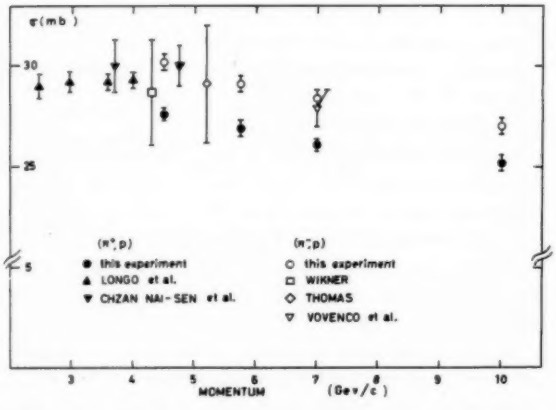

FIG. 2. Total cross sections for (π^-,p) and (π^+,p) versus momentum. Observe break in ordinate scale.

The difference observed between the cross sections for negative and positive pions is outside the errors, and slowly decreasing with increasing energy. This difference may be due to elastic charge exchange of negative pions, but should vanish if the equality of the cross sections in different isotopic spin states, predicted by Pomeranchuk's theorem, were fulfilled. That it does not vanish confirms the conclusion of the preceding paragraph.

The monotonic decrease of the cross sections at high energies could, if it continued, be considered in connection with recent theories by Berestetsky and Pomeranchuk[9] and Gribov[10] which suggest a cross section decreasing to zero faster than $(\ln E)^{-1}$. Extrapolating our values according to the functional dependence $\sigma = \sigma_0[\ln(E/E_0)]^{-1}$ leads to cross sections of 20 mb at 100 Gev and 16 mb at 1000 Gev.

We are indebted to the Machine Group of the CERN Proton Synchrotron for the efficient operation of the machine during the whole run. We also thank M. Rousseau and L. Velati for their assistance in setting up and running the experiment.

---

*Present address: Palmer Physical Laboratory, Princeton University, Princeton, New Jersey.

[1]G. von Dardel, D. H. Frisch, R. Mermod, R. H. Milburn, P. A. Piroué, M. Vivargent, G. Weber, and K. Winter, Phys. Rev. Letters 5, 333 (1960).

[2]I. Pomeranchuk, J. Exptl. Theoret. Phys. (U.S.S.R.) 34, 725 (1958) [translation: Soviet Phys.-JETP 34(7), 499 (1958)].

[3]M. J. Longo, J. A. Helland, W. N. Hess, B. J. Moyer, and V. Perez-Mendez, Phys. Rev. Letters 3, 568 (1959).

[4]F. Wikner, thesis, University of California Radiation Laboratory Report UCRL-3639, 1957 (unpublished).

[5]R. G. Thomas, University of California Radiation Laboratory Report UCRL-8965, 1959 (unpublished).

[6]A. S. Vovenko, B. A. Kulakov, A. L. Lubimov, Y. A. Matulenko, I. A. Savin, E. V. Smirnov, and M. D. Shafranov, Proceedings of the 1960 Annual International Conference on High-Energy Physics at Rochester (Interscience Publishers, Inc., New York, 1960), p. 433.

[7]Chzan Nai-sen, Sui Yuin-chan, M. F. Lykhachev, and V. S. Stavinsky, Proceedings of the 1960 Annual International Conference on High-Energy Physics at Rochester (Interscience Publishers, Inc., New York, 1960), p. 444.

[8]A. Ashmore, G. Cocconi, A. N. Diddens, and A. M. Wetherell, Phys. Rev. Letters 5, 576 (1960).
[9]V. B. Berestetsky and I. Pomeranchuk, Proceedings of the 1960 Annual International Conference on High-Energy Physics at Rochester (Interscience Publishers, Inc., New York, 1960), p. 333.
[10]V. N. Gribov, Proceedings of the 1960 Annual International Conference on High-Energy Physics at Rochester (Interscience Publishers, Inc., New York, 1960), p. 340.

MAGNETIC MOMENT OF POSITIVE AND NEGATIVE MUONS*

D. P. Hutchinson, J. Menes,† and G. Shapiro
Columbia University, New York, New York

A. M. Patlach
International Business Machines Watson Scientific Computing Laboratory, New York, New York

and

S. Penman‡
University of Chicago, Chicago, Illinois

(Received July 24, 1961)

This Letter reports on the refinement of the technique for measuring muon magnetic moments and on its application to positive and (bound) negative muons in various materials. These refinements enable us to obtain a statistical accuracy of several parts per million in reasonably short runs. In addition to the absolute measurement of g_μ, this sensitivity permits the observation of environmental effects and thus has applications to nuclear and solid-state physics.

The magnetic moment of the μ meson, like that of the electron, is of theoretical importance because of the exact predictions that can be made of its magnitude. Quantum electrodynamics enables one to calculate the moment[1] in units of the muon magneton, $e\hbar/m_\mu c$. *TCP* invariance requires the positive and negative muon, as particle and antiparticle, to have equal magnetic moments.[2]

Since the discovery of parity nonconservation, there has been a succession of increasingly accurate measurements[3-5] of the muon magnetic moment, at this laboratory and elsewhere. These experiments, as well as the present one, generally express the muon moment in units of the proton magnetic moment, and depend on separate determinations of the muon mass[6] for comparison with theory. A direct measurement of the "anomalous part" of the magnetic moment, which does not depend strongly on the mass value for its interpretation, has also recently been made.[7] The accuracy of the present experiment so far exceeds that of any muon mass determination that it must await future experiments on the latter before its significance can be realized. Alternatively one can accept present theoretical[1] or experimental[7] estimates of the g factor, and combine them with the present results to obtain a "best" value for the muon mass.

The basic method of this experiment is similar to that of reference 5, to which the reader is referred for details. The increased sensitivity of the present experiment is due to numerous improvements in the apparatus, including a higher muon precession frequency, an extremely homogeneous magnetic field, and the transistorizing of all circuitry. Recent improvements in the beam facilities at Nevis, including the long-duty-cycle beam and a new low-energy muon beam, also contributed to the increased sensitivity. Figure 1 shows the experimental arrangement.

Figure 2 shows the results of typical runs with positive and negative muons stopping in HCl solution and graphite, respectively. Early-late phase shift is plotted against magnetic field, as measured by a proton magnetic resonance[8] at the monitor position. Experimental conditions were such that for a target material that does not depolarize positive muons (e.g., bromoform), running time of three hours was sufficient to reduce the statistical error to 12 ppm.

Results of the runs with positive muons stopping in various target materials are summarized in Table I, in chronological order. Statistical errors calculated from a priori considerations are indicated.

The accuracy of the experiment is such that diamagnetic shielding of the muon by atomic elec-

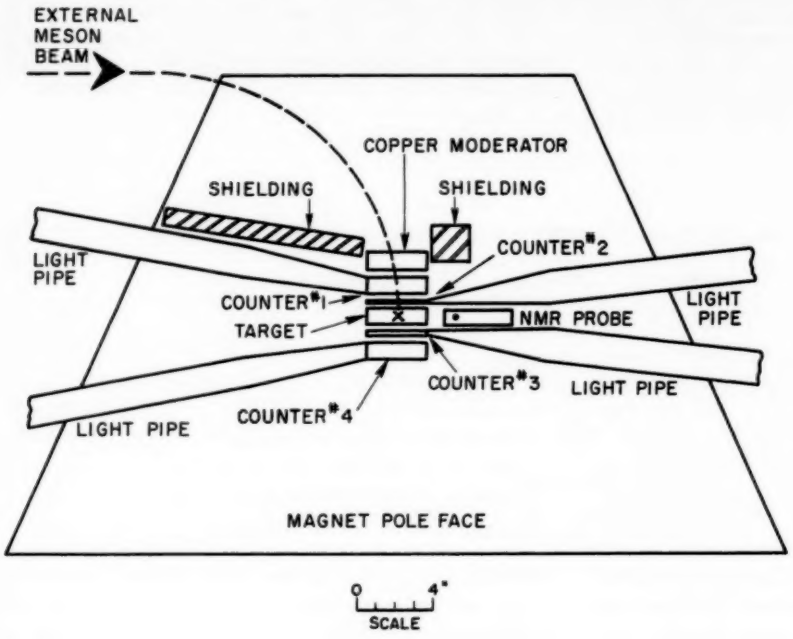

FIG. 1. Experimental arrangement. The meson beam from the Nevis cyclotron enters at the left, and is brought to rest in the target. Decay electrons emitted into counters No. 3 and No. 4 are analyzed.

Table I. Results for positive muons. Errors indicated are statistical only.

Stopping material	Proton frequency at resonance (kc/sec)	
Methylene iodide $-CH_2I_2$	55 824.45	±0.49
Distilled water $-H_2O$	55 823.41	±0.49
HCl	55 822.07	±0.35
H_2O – repeat	55 821.39	±0.94
Methylene iodide – repeat	55 823.33	±0.59
Bromoform	55 823.30	±0.69
Average	55 823.01	±0.43
Monitor-to-center field difference	-4.85	±0.10
	55 818.16	
Muon precession frequency at resonance	177 688.4	±0.1
f_μ/f_p	3.18334	±0.00005
μ^+ in graphite (99.995% pure electromolded)	55 801.8	±1.8

trons must be considered. If the positive muon substitutes immediately for a proton and experiences the same shielding, the shifts are expected to be less than 3 ppm (relative to a proton in water) for all liquid targets used.[9] The proton resonance for measuring the field is also taken in aqueous solution, so essentially no net correction has to be made for the ratio of the moments.

It is noted that the substituted hydrocarbons yield consistently higher values than the aqueous targets, beyond the predictions of chemical shifts. Moreover, there is a downward trend with time for runs repeated with the same type of target. Rigorous checks of the system gave no evidence for a systematic drift in this direction. Therefore, it is assumed that both these effects are statistical fluctuations and the error is increased to account for the observed spread.

The average proton resonance frequency thus obtained is 55823.01 ± 0.43 kc/sec. From this

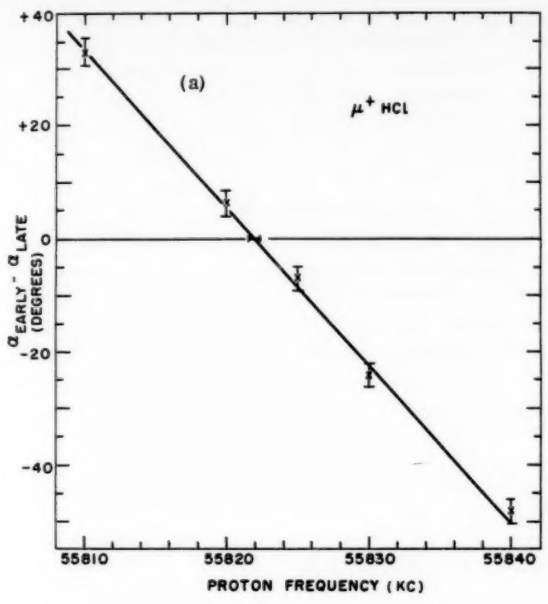

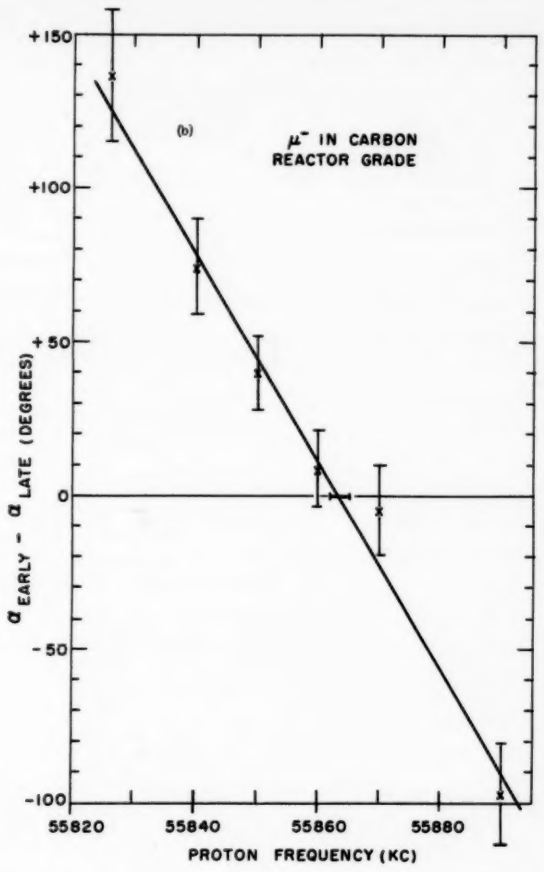

FIG. 2. Early-late phase shift vs proton resonance frequency at monitor position. The straight line is the least-squares best fit, crossing the x axis at the field setting where the muon precession frequency equals the reference value. The horizontal flag at this point is a calculated a priori statistical error. (a) Positive muons in HCl solution; (b) negative muons in graphite (reactor grade).

must be subtracted 4.85 ± 0.10 kc/sec as the difference between the field measured at the monitor position and at the center of the target. The muon precession frequency at "resonance" is 177 688.4 ± 0.1 kc/sec. An improved transistor regulator[10] permits maximum excursions of less than 5 ppm in the field setting (~13.4 kgauss) during each one-hour run. Field spatial homogeneity is such that the maximum deviation from the average over 95% of the target volume (2 in.×3 in.×1 in.) is not more than 10 ppm. The result for positive muons is $f_\mu/f_p = 3.18334 \pm 0.00005$, where the error has been increased to allow for possible systematic errors.

Similar measurements have been made on the magnetic moment of the electron. The most accurate experimental result to date is[11] $f_e/f_p = 658.22759 \pm 0.00004$, as the ratio of the spin precession frequency of free electrons to that of protons in water. Since in the present experiment both muon and proton are bound, a correction[12] for diamagnetic shielding of 25.6 ppm must be made to one of these results before they can be compared. Making it to the electron experiment yields f_e/f_p(both free) = 658.2107, with an error small compared to that of the muon result. These frequencies are proportional to the g factors of the particles, and inversely to their masses. For the ratio of the g factors, one can use either the theoretical value, $g_\mu/g_e = 1.000006$;[1] or the experimentally determined g factors, $g_\mu = 1.001145 \pm 0.000022$,[7] and $g_e = 1.0011609 \pm 0.0000024$.[13] Using the theoretical g factor, one obtains for the ratio of the masses $m_\mu/m_e = 206.768 \pm 0.003$. Using the experimental numbers, one has $m_\mu/m_e = 206.763 \pm 0.005$. The larger error in the latter case reflects the effect of folding in the error in the result of Charpak et al. with that of this experiment. The average of the mesonic x-ray determinations of the mass[6] yields $m_\mu/m_e = 206.76 \pm 0.02$, in excellent agreement with the above, but not sufficiently

Table II. Results for negative muons. Errors indicated are statistical only.

Z	Stopping material	Proton frequency at resonance (kc/sec)	$\left(\frac{g-g^+}{g^+}\right)\times 10^4$	Theoretical corrections ($\times 10^4$) Direct binding[a]	Binding effect on radiative correction[a]	Nuclear polarization[a]	Diamagnetic shielding[b]	Knight shift[c]	Total
μ^+	(corrected for diamagnetism)	55 821.5 ± 0.5							
6	Graphite, reactor grade	55 863.4 ± 1.7	- 7.5 ± 0.3	- 6.29	-0.08	+0.04	-1.99	?	- 8.32
6	Graphite, 99.995% pure, 300°K	55 860.5 ± 3.1	- 6.9 ± 0.6	- 6.29	-0.08	+0.04	-1.99	?	- 8.32
6	Graphite, 99.995% pure, 77°K	55 865.7 ± 2.7	- 7.9 ± 0.5	- 6.29	-0.08	+0.04	-1.99	?	- 8.32
8	Oxygen in water	55 873.7 ± 5.7	- 9.3 ± 1.0	-11.04	-0.13	+0.12	-3.25	0	-14.30
12	Magnesium	55 968.5 ± 3.7	-26.3 ± 0.7	-23.79	-0.29	+0.53	-6.29	?	-29.84
14	Silicon 300 ohm cm, n type	56 023.5 ± 6.0	-36.1 ± 1.1	-31.72	-0.40	+0.90	-7.95	?	-39.17
16	Sulfur	56 090.0 ± 9.1	-48.1 ± 1.6	-40.35	-0.51	+1.4	-9.70	0	-49.16

[a] See reference 17.
[b] See reference 19.
[c] See reference 15.

accurate to afford a real comparison.

A run was made with positive muons stopping in graphite. As noted in Table I, there is a paramagnetic shift of about 400 ppm from the average of the liquid targets. A similar (but smaller) shift was earlier[14] noted in copper and aluminum, and was then interpreted as a Knight shift.[15] No other explanation of this effect is known to the authors; further investigations are being made. The graphite result was not used in the average for the positive muons.

The results for negative muons stopping in various target materials are tabulated in Table II. These muons are observed in the ground state of mesonic atoms formed with the nuclei listed, and corrections must be made in order to compare with positive muons. The largest correction is due to binding.[16] The statistical error on the data requires that the finite nuclear radius be taken into account in calculating this correction for $Z \geq 12$. This experiment thus offers another way of probing the nucleus. The numbers quoted in Table II are from Ford, Hughes, and Wills.[17]

The next largest correction to be applied to negative muons is due to diamagnetic shielding at the nucleus by the bound electrons.[18] Because of uncertainty in the final electronic states, Dickinson's[19] results for atomic number Z-1 have been quoted without modification, although his results are for neutral isolated atoms. The magnitude of the effect is sufficient for this experimental method to provide a determination of the absolute shielding.

Several smaller corrections taken from Ford, Hughes, and Wills[17] are also listed in Table II. No entries have been made under "Knight shift" for carbon, magnesium, and silicon. We hope to have soon a measurement of Knight shift in our carbon samples. The Knight shift in magnesium, expected to be a few parts in 10^3, would predict a result in great disagreement with the data. A search was made for a "resonance" in the predicted region, with negative results. There exists a result for the Knight shift in silicon.[20] However, the shift may be sensitive to the doping of the sample, and therefore this result has not been used.

The negative-muon results are less accurate than those for positive muons because of depolarization and, for higher Z, shorter lifetime.

Table II shows reasonable agreement between

predicted and measured muon moments in all the atoms investigated. It is concluded that, allowing also for theoretical uncertainties, the magnetic moment of positive and negative free muons are equal to within five parts in 10^4. It may be that the various shifts mentioned will become a subject for investigation in their own right, the muon serving as a tool for probing them.

We wish to thank our respective sponsors, Professor A. M. Sachs, Professor L. M. Lederman, and Professor R. L. Garwin for their encouragement and support. We also thank W. Blumberg, J. Eisinger, and S. Geschwind of Bell Telephone Laboratories for a useful discussion on Knight shift, and K. Ford, V. Hughes, and J. G. Wills for a preprint of their paper.

---

*This research was supported in part by the Office of Naval Research.

†Dupont Fellow.

‡Present address: Marine Biological Laboratory, Wood's Hole, Massachusetts.

[1]H. Suura and E. H. Wichmann, Phys. Rev. 105, 1930 (1957); A. Petermann, Phys. Rev. 105, 1931 (1957).

[2]H. Rubinstein (private communication).

[3]T. Coffin, R. L. Garwin, S. Penman, L. M. Lederman, and A. M. Sachs, Phys. Rev. 109, 973 (1958).

[4]R. A. Lundy, J. C. Sens, R. A. Swanson, V. L. Telegdi, and D. D. Yovanovitch, Phys. Rev. Letters 1, 38 (1958).

[5]R. L. Garwin, D. P. Hutchinson, S. Penman, and G. Shapiro, Phys. Rev. 118, 271 (1960).

[6]J. Lathrop, R. A. Lundy, V. L. Telegdi, R. Winston, and D. D. Yovanovitch, Nuovo cimento 17, 109 (1960); J. Lathrop, R. A. Lundy, S. Penman, V. L. Telegdi, R. Winston, D. D. Yovanovitch, and A. J. Bearden, Nuovo cimento 17, 114 (1960); S. Devons, G. Gidal, L. M. Lederman, and G. Shapiro, Phys. Rev. Letters 5, 330 (1960).

[7]G. Charpak, F. J. M. Farley, R. L. Garwin, T. Muller, J. C. Sens, V. L. Telegdi, and A. Zichichi, Phys. Rev. Letters 6, 128 (1961).

[8]"Numar" Yellow Probe No. 154A, manufactured by Nuclear Magnetics Corporation, 154 Boylston Street, Boston 16, Massachusetts.

[9]J. A. Pople, W. G. Schneider, and H. J. Bernstein, High-Resolution Nuclear Magnetic Resonance (McGraw-Hill Book Company, Inc., New York, 1959), p. 279 and p. 443.

[10]A. M. Patlach, IBM Internal Report No. RW 19, an abridged version of which appears in Electronics 33, 66 (1960).

[11]See J. W. M. DuMond, Ann. Phys. 7, 365 (1959).

[12]Reference 9, pp. 90, 169, and 403. See this book for other references.

[13]A. A. Schupp, R. W. Pidd, and H. R. Crane, Phys. Rev. 121, 1 (1961).

[14]R. L. Garwin, D. P. Hutchinson, S. Penman, and G. Shapiro, Phys. Rev. Letters 2, 213 (1959).

[15]W. D. Knight, Solid-State Physics, edited by F. Seitz and D. Turnbull (Academic Press, New York, 1956), Vol. II, p. 93.

[16]H. Margenau, Phys. Rev. 57, 383 (1940).

[17]K. Ford, V. W. Hughes, and J. G. Wills, following Letter [Phys Rev. Letters 7, 134 (1961)].

[18]W. E. Lamb, Jr., Phys. Rev. 60, 817 (1941).

[19]W. C. Dickinson, Phys. Rev. 80, 563 (1950).

[20]H. E. Weaver, Jr., Phys. Rev. 89, 923 (1953).

THEORETICAL VALUES FOR MAGNETIC MOMENTS OF μ-MESONIC ATOMS*

Kenneth W. Ford
Brandeis University, Waltham, Massachusetts

Vernon W. Hughes
Yale University, New Haven, Connecticut

and

John G. Wills†
Los Alamos Scientific Laboratory, Los Alamos, New Mexico

(Received July 24, 1961)

Precise measurements of the magnetic moments of negative μ mesons bound in μ-mesonic atoms are reported in the preceding Letter. Theoretical calculations of the magnetic moments of μ-mesonic atoms are outlined and summarized in this Letter.

It has been pointed out that the magnetic moment (or g value) of a negative muon bound in an atomic orbit about a nucleus will be slightly less than that of a free muon and that the magnitude of this alteration is sensitive to the size of the nucleus.[1] The corrections to the gyromagnetic ratio of a Dirac particle ($g_0 = 2$) bound in the field of a zero-spin nucleus and surrounded by a zero-spin electronic cloud may be listed as follows:

1. radiative correction, g_1;
2. binding correction to radiative correction, g_2;
3. direct binding correction, g_3;
4. nuclear polarization correction, g_4;
5. electronic polarization correction, g_5;
6. electronic diamagnetic shielding correction, g_6;
7. center-of-mass correction, g_7.

We consider that the muon is bound in a 1s orbit about the nucleus.

The radiative correction[2] and the binding correction[3] thereto have already been calculated:

$$g_1/g_0 = \alpha/2\pi + 0.75(\alpha/\pi)^2 = 0.001165, \quad (1)$$

$$g_2/g_0 = (26/15\pi)\alpha\langle V\rangle/mc^2, \quad (2)$$

where $\langle V\rangle$ is the expectation value of the potential energy and m is the muon mass. The direct binding correction, g_3, is computed from a relativistic treatment of the magnetic moment of a Dirac particle in a central field.[4] The result is

$$g_3/g_0 = -(4/3)\int F^2 dr, \quad (3)$$

where F is the small component of the radial wave function of the muon in the Coulomb field of a nucleus with finite size. Both the corrections g_2 and g_3 have been obtained from the relativistic bound-state muon wave functions calculated on an IBM-704 computer. The nuclear charge distribution is taken to be

$$\rho(r) = (Ze/4\pi r_1^3 N_0)\left(1 - \tfrac{1}{2}e^{-n(1-x)}\right) \text{ for } x < 1,$$

$$= (Ze/4\pi r_1^3 N_0)\left(\tfrac{1}{2}e^{-n(x-1)}\right) \text{ for } x \geq 1, \quad (4)$$

where $x = r/r_1$ and

$$N_0 = \tfrac{1}{3} + 2n^{-2} + n^{-3}e^{-n}.$$

The parameters r_1 and n, which characterize the nuclear radius and surface thickness, were chosen to be those which have been used to fit high-energy electron scattering results.[5] The effect of the nuclear size on g_3 is significantly larger than the experimental error for $Z \geq 12$.

A significant nuclear polarization correction term, g_4, arises in second order perturbation theory from the magnetic interaction between the muon and the nucleus together with the magnetic interaction of the nucleus in the external static magnetic field. In an approximate calculation the term g_4 can be related to $M1$ nuclear gamma transition rates. An electronic polarization correction term, g_5, arises in second order perturbation theory from the magnetic interaction between the muon and the electrons together with the magnetic interaction of the electrons in the external static magnetic field.[6] The correction term g_5 is negligible unless the ground electronic state has fine-structure levels.

The usual diamagnetic shielding[7] by the atomic electrons will be very nearly the same for the muon as it is for the nucleus. This effect can be expressed by a correction term, g_6:

$$g_6/g_0 = -\tfrac{1}{3}\alpha^2\textstyle\sum_i\langle a_0/r_i\rangle,$$

in which the sum is taken over all the electrons. The center-of-mass correction g_7 is negligibly small.

Table I. Calculated corrections to the g values of selected μ-mesonic atoms.

Element	g_1/g_0	g_2/g_0	g_3/g_0 [a]	g_4/g_0	g_6/g_0	g/g_0 [b]	$(g-g_{\mu+})/g_0$
$_6$C	0.001165	-0.000008	-0.000629(0)	+0.000004	-0.00019	1+0.00034	-0.00082
$_8$O	0.001165	-0.000013	-0.001104(1)	+0.000012	-0.00032	1-0.00026	-0.00143
$_{12}$Mg	0.001165	-0.000029	-0.002379(6)	+0.000053	-0.00062	1-0.00181	-0.00298
$_{14}$Si	0.001165	-0.000040	-0.003172(10)	+0.000090	-0.00079	1-0.00275	-0.00391
$_{16}$S	0.001165	-0.000051	-0.004035(15)	+0.00014	-0.00096	1-0.00374	-0.00491

[a] Numbers in parentheses are uncertainties arising from 2% uncertainty in nuclear radius.
[b] The quantity $g \equiv \sum_{i=0}^{6} g_i$.

Table I lists the significant corrections for the elements measured experimentally. The terms g_5 and g_6 depend on the electronic state of the μ-mesonic atom. For the elements listed, binding-energy considerations suggest that the μ-mesonic atoms will be positive ions with Z-2 electrons and the electronic states will be $^1S_0$ except for oxygen and sulfur which will be $^3P_0$. The diamagnetic shielding term g_6 is obtained from Dickinson's value[8] for an atom with Z-1 electrons together with a small estimated correction to give g_6 for the positive ion. The term g_5 will be negligible except for oxygen and sulfur where it amounts to about 5% and 2%, respectively; it is not included in the table since the large theoretical values for O and S are clearly inconsistent with the experimental values, thus indicating that the atomic states are not simple $^3P_0$ states.

In view of uncertainties about the electronic state of the μ-mesonic atom (the state might even have electronic angular momentum J nonzero and then the hfs interaction between muon and electrons would be important), about chemical effects,[9] and about solid-state effects such as the Knight shift,[10] the agreement between theory and experiment is close. The chemical shift and the Knight shift are paramagnetic effects, having the same sign as that required to account for the small remaining discrepancies. There is no indication for any anomalous behavior of the muon such as its polarization in the strong electric field of the nucleus.

A more detailed report on these theoretical calculations will be submitted to The Physical Review.

---

*This research has been supported in part by the U. S. Atomic Energy Commission, the National Science Foundation, and the Air Force Office of Scientific Research and Development.

†Now at University of Washington, Seattle, Washington.

[1]V. W. Hughes and V. L. Telegdi, Bull. Am. Phys. Soc. 3, 229 (1958); K. W. Ford, V. W. Hughes, and J. G. Wills, Bull. Am. Phys. Soc. 6, 268 (1961).
[2]C. M. Sommerfield, Ann. Phys. 5, 26 (1958).
[3]E. H. Lieb, Phil. Mag. 46, 311 (1955).
[4]G. Breit, Nature 122, 649 (1928).
[5]U. Meyer-Berkhout, K. W. Ford, and A. E. S. Green, Ann. Phys. 8, 119 (1959).
[6]W. W. Clendenin, Phys. Rev. 94, 1590 (1954).
[7]W. E. Lamb, Jr., Phys. Rev. 60, 817 (1941).
[8]W. C. Dickinson, Phys. Rev. 80, 563 (1950).
[9]N. F. Ramsey, Nuclear Moments (John Wiley & Sons, New York, 1953), p. 71.
[10]W. D. Knight, Solid-State Physics, edited by F. Seitz and D. Turnbull (Academic Press, New York, 1956), Vol. 2, p. 93.

EXAMPLE OF THE DECAY $\Lambda^0 \to p + \mu^- + \bar{\nu}$*

F. Eisler, J. M. Gaillard,† J. Keren, M. Schwartz,‡ and S. Wolf
Columbia University, New York, New York, and Brookhaven National Laboratory, Upton, New York
(Received July 25, 1961)

The decay $\Lambda^0 \to p + \mu^- + \bar{\nu}$, while expected, has not yet been reported to the knowledge of the authors. We report here a clear case of such a decay found in an exposure taken in the 20-in. BNL hydrogen bubble chamber.

The exposure was taken in a carefully constructed π^- beam of energy 900 Mev and resolution 0.15%. The beam energy has been further confirmed by the analysis of over 1000 normal $\Lambda^0 K^0$ events. A picture of the event is shown in Fig. 1. The incident beam track, (1), interacts at a position 13 cm inside the chamber entrance which corresponds to an energy of 900 Mev. The Λ^0, (2), goes 5.6 cm before decaying, a distance less than 2 mean lives. Track (3) is a proton. The μ^-, track (4), goes 9.6 cm before coming to rest and decaying into an electron, (5), which leaves the chamber through the top window.

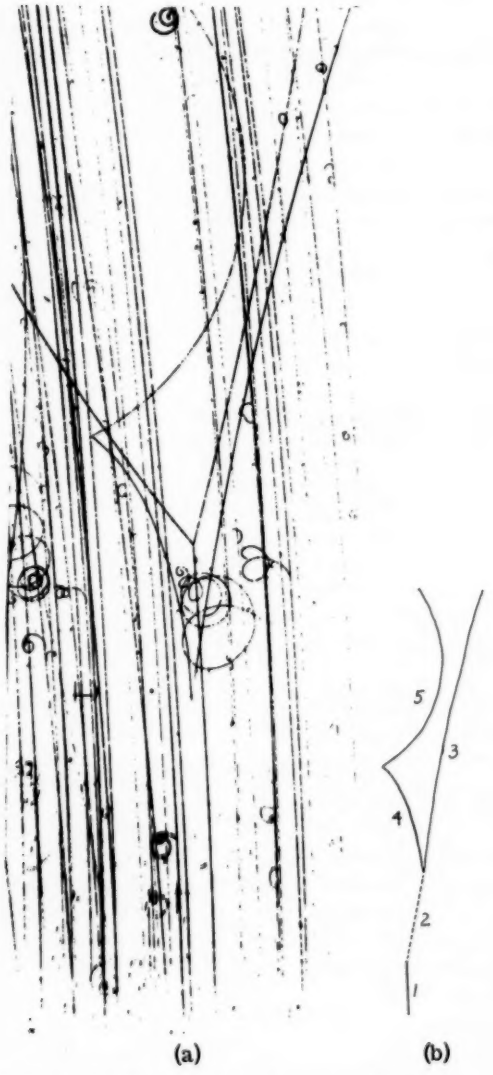

FIG. 1. (a) Photograph of the event. (b) Tracing of the pertinent tracks (reduced).

Four views of the event are available and were used in the measurement. The measurements and assigned errors are given in Table I.

From the production angle of $16° \pm 0.8°$ and known beam energy, the Λ^0 momentum is 495^{+15}_{-10} Mev/c. Under the assumption of the decay $\Lambda^0 \to p + \mu^- + \bar{\nu}$, the calculated neutrino energy from momentum balance is 79 ± 15 Mev/c, giving a total final Λ^0 energy of 1223 Mev $\pm$ 20 Mev from summing the energy of its decay products. This energy and the momentum taken above, yield a mass for the Λ^0 of 1118 ± 21 Mev, in good agreement with the known Λ^0 mass.

The competing decay sequence $\Lambda^0 \to \pi^- + p$, $\pi^- \to \mu^- + \bar{\nu}$ is found to be very unlikely. The major points against this interpretation are as follows:

(a) The proton momentum would have to be 475 ± 20 Mev/c for this interpretation to hold. It is measured as 412 ± 20 Mev/c.

(b) If one assumes a pion to have been produced, then its direction would have been such as to make too large an angle with the μ, by about twice the measurement error.

(c) There is less than 1 mm of possible flight path for the π^- since no sign of it is detected visually. The mean decay path for a π^- with the required energy would be 5 meters.

The above combine to give this interpretation a probability of occurrence of the order of less than 10^{-5}.

Other possibilities for this event are:

(1) It originates at the wall of the chamber, rather than at the observed pion ending. It would have had to travel 5 mean lives before decay.

(2) The Λ^0 scatters in the chamber before decay, with no visible recoil.

Each of these possibilities seems even more remote than the one previously explored since

Table I. Summary of measured data.

Tracks	Length measured (cm)	Azimuth (deg)	Dip (deg)	Momentum (Mev/c)
$(\pi^-)_{in}$ (1)	2.5	62.5 ± 0.5	89.8 ± 1.0	1030 ± 2
Λ^0 (2)	5.6	50.6 ± 0.2	100.8 ± 0.4	495^{+15}_{-10}[a]
P (3)	23.0	56.3 ± 0.3	110 ± 0.4	412 ± 20
μ (4)	9.4	50.8 ± 1.5	40.5 ± 1.5	56 ± 1 (range)

[a]Fitted quantity.

one must still require the decay of the pion within 1 mm.

From these different results, we conclude that this event has to be interpreted as a muonic decay of the Λ^0 particle. Theoretically, the rate for this decay mode is predicted to be 2.4×10^{-3}.[1]

The above-described event is one of a sample of 3000 Λ^0's presently being analyzed. Our systematic study of these events has as yet not been completed and we cannot set an upper limit on the rate of the decay.

We would like to express our gratitude to Dr. J. Steinberger for valuable discussions. We would also like to thank Dr. R. Shutt and the members of the BNL Bubble Chamber Group for their invaluable aid in obtaining the pictures and Mrs. Frances Joyce for having found the event.

---

*Work was supported by the U. S. Atomic Energy Commission.

†On leave of absence from Centre d'Etudes Nucleaires de Saclay, Seine et Oise, France.

‡Alfred P. Sloan Research Fellow.

[1]See, for example, L. Okun', Ann. Rev. Nuclear Sci. 9, 61 (1959).

CHARGE ASYMMETRIES IN THE ANGULAR DISTRIBUTION OF π AND K MESONS FROM ANTIPROTON ANNIHILATIONS IN FLIGHT

B. C. Maglić, G. R. Kalbfleisch, and M. L. Stevenson
Lawrence Radiation Laboratory, University of California, Berkeley, California
(Received July 27, 1961)

Presented here are the results of our search for a difference in the angular distributions of negative and positive π and K mesons produced in $\bar{p}p$ annihilations, at the center-of-mass momentum of 657 ± 16 Mev/c (1.6 Bev/c in the lab). There have been no direct theoretical predictions for such a difference. The statistical model prescribes an isotropic distribution for mesons of all charges.[1] However, the model of Koba and Takeda[2] assumes that 2 or 3 annihilation pions are emitted from the antiproton and proton clouds. For annihilations in flight, the instantaneous momentum of the pions from the $\bar{p}$ cloud will have a component parallel to the $\bar{p}$ momentum, in addition to their internal momenta. Since the model assumes that the pion cloud does not interact with the annihilation of the cores, it is reasonable to expect this component of the pion momentum to produce an excess of π^- over π^+ in the antiproton direction (forward). An equal excess of π^+ should also be expected in the direction of the proton (backward). Evidence for such an effect has been scarce prior to this experiment. Angular distributions of pions of both charges from $\bar{p}p$ annihilations in propane at a c.m. momentum of 470 Mev/c (1.05 Bev/c lab) have not shown statistically significant deviation from isotropy.[3] A study of $\bar{p}p$ annihilations into two pions[4] at our momentum is also consistent with an isotropic distribution (8 π^- emitted forward, and 12 π^- emitted backward). However, annihilations into K^+K^- pairs[4] suggest forward peaking for K^- (8 of the 11 K^- were emitted in the forward direction).[5]

Our analysis was done on two samples of events: (i) 1620 events of the type $\bar{p}+p\rightarrow n\pi$, with $n=4, 5, \ldots, 8$; and (ii) 287 events of the type $\bar{p}+p\rightarrow\bar{K}+K+n\pi$, with $n=1, 2, 3$, and $4-$ in which at least one of the K mesons was observed to decay in the chamber. These events were observed inside a central volume of the 72-in. hydrogen bubble cham-

ber. The average antiproton momentum at the point of interaction was 1.61 ± 0.04 Bev/c (925-Mev kinetic energy) for Sample (i), and for 86% of Sample (ii). The remaining 14% of Sample (ii) was from our run at 1.99 ± 0.05 Bev/c. The experimental conditions have been described previously.[5]

(i) Reactions $\bar{p}+p \to n\pi$. Only annihilations into 4 prongs have been analyzed, in which the identifiable reactions are

$$\bar{p}+p \to 2\pi^- + 2\pi^+ + \pi^0, \quad (1)$$

and

$$\bar{p}+p \to 2\pi^- + 2\pi^+. \quad (2)$$

The abundances of these reactions are about 50% and 10%, respectively. Competing reactions,

$$p+p \to 2\pi^- + 2\pi^+ + n\pi^0, \quad (3)$$

occur with frequencies of about 32%, 7%, and 1% for $n=2$, 3, and 4, respectively.

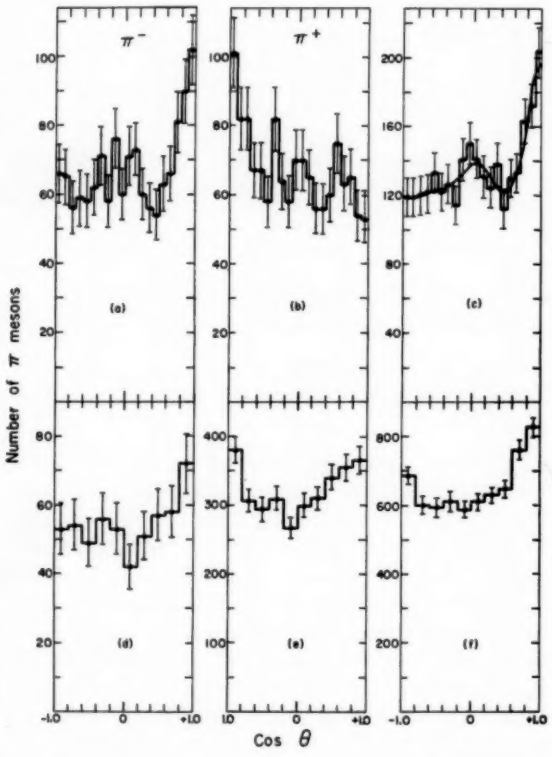

FIG. 1. Histograms of c.m. angular distribution of pions from Reactions (1) to (3). (a) and (b): π^- and π^+ from Reaction (1); (c): combined distributions (a) plus reflected (b); (d): π^- and reflected π^+ from Reaction (2); (e): negative and reflected positive prongs which did not fit Reactions (1) and (2); and (f): combined data (c), (d), and (e). The forward-to-backward ratio, F/B, is 1.17 ± 0.04, 1.06 ± 0.09, 1.08 ± 0.04, and 1.13 ± 0.03 for distribution (c), (d), (e), and (f), respectively.

The dynamical fit for each event was done by using an IBM-709 computer program (KICK).[6] The probability of a background reaction $\pi^- + p \to 4$ prongs being wrongly identified as either Reaction (1) or (2) is negligibly small. When the prongs are wrongly transformed into the $\bar{p}p$ c.m. system as pions, there is much too little visible energy and, consequently, several missing π^0's are required in order to conserve both momentum and energy. Secondly, the pion contamination in the $\bar{p}$ beam was 36%, and the pion cross section for producing 4-prong stars small, namely, about 2.5 mb compared with 15 mb for $\bar{p}+p \to 4$ prongs.

Reaction $\bar{p}+p \to 2\pi^- + 2\pi^+ + \pi^0$. We identified 674 cases of Reaction (1). These events satisfied the following conditions: (a) The χ^2 for the hypothesis (1) was ≤ 9; (b) the value of the missing mass of 4 prongs, interpreted as pions, was within 2.5 standard deviations of 135 Mev; (c) the fitted $\bar{p}$ momentum was > 640 Mev/c; and (d) there was no fit for hypothesis (2). Of this sample, 410 events (60%) had $\chi^2 \leq 2.5$ and a missing mass < 250 Mev. The still-unresolved systematic errors of our measuring system produce an extended tail in the χ^2 distribution, so that the cutoff value of χ^2 has to be increased generally by a factor of two or three. The angular and momentum distributions of the pions did not show any substantial difference between the samples with $\chi^2 < 2.5$ and $\chi^2 < 9$. Our confidence is increased by the fact that the momentum distribution of π^0's agrees very well with that of charged π's.

The c.m. angular distribution for Reaction (1) is shown separately for π^- and π^+ in Figs. 1(a) and 1(b). The π^- distribution displays a forward peak, whereas that of the π^+ is backward, contrary to the statistical model. As expected on the basis of C and CP,[7] the distribution of π^+ appears to be equal, within statistics, to the reflection of the angular distribution of the π^-'s. To analyze the shape of the distribution, we have reflected the π^+ distribution about $\cos\theta = 0$ and added it to the π^- distribution [Fig. 1(c)]. We have found it convenient (without inquiring into its physical meaning) to express our distribution in terms of the expansion $\sum a_l P_l(\cos\theta)$, where P_l are Legendre polynomials and the coefficients are (in units of numbers of pions): $a_0 = 135.3 \pm 2.2$, $a_1 = 24.1 \pm 3.9$, $a_2 = 18.2 \pm 5.1$, $a_3 = 24.4 \pm 6.1$, $a_4 = 19.4 \pm 7.1$, a_5

$=10.0\pm 8.9$, $a_6=-14.3\pm 8.9$, and $a_7=-10.2\pm 10.1$. Note that the sharpness of the distribution makes the fourth order polynomial at least essential for describing the observed effect. The angular distribution of the π^0's does not show statistically significant deviations from isotropy. The momentum distribution of all charged pions agrees well with the phase space distribution, which predicts an average momentum $\langle K\rangle_{\rm av}=439$ Mev/c. However, for π^- (π^+) emitted in forward (backward) cone with $|\cos\theta|\geq 0.70$, we observe $\langle K\rangle_{\rm av}=451\pm 10$ Mev/c, whereas for the nonforward pions it is 427 ± 7 Mev/c. For those events that have simultaneously a π^- (π^+) in the forward and a π^+ (π^-) in the backward cone, $\langle K\rangle_{\rm av}=495\pm 15$ Mev/c (482 ± 26). It is interesting to note that the hydrodynamic model of multiple-pion production in nucleon-nucleon collisions[8] predicts an increase of pion momenta at small angles.

To determine whether the like pions ($\pi^+\pi^+$ or $\pi^-\pi^-$) have a tendency to be emitted in pairs in the forward peak [Fig. 1(c)], we have counted the number of Reaction (1) in which both π^-'s have $\cos\theta\geq 0.80$ (≤ -0.80 for $\pi^+\pi^+$). If the probability of finding the second π^- in this angular interval were independent of finding the first π^- in this interval, then the probability that both π^- mesons would be found there would be $1.9\pm 0.1\%$.[9] We observe simultaneous forward (backward) emission of pairs of π^- (π^+) in 15 cases of Reaction (1), or $2.2\pm 0.6\%$.

It has been reported that the angles between the like pions produced in annihilation are smaller on the average than the values predicted by the phase space.[10] Our data confirm this observation. The phase space predicts a value of 1.79 for the ratio $\gamma=$(number of pion pairs with angle $>90°$):(number of pion pairs with angle $<90°$), whereas we observe $\gamma=1.56\pm 0.08$ for like pions. To find out whether or not this is caused, in part, by our angular distribution characterized by the sharp peak, we have evaluated γ for only those pairs in which at least one π^- has $\cos\theta\geq 0.80$ (≤ -0.80 for π^+), and obtained $\gamma=1.38\pm 0.13$. For comparison, we have also evaluated γ for the pairs in which at least one π^- has $\cos\theta\leq -0.80$ (≥ 0.80 for π^+) and obtained $\gamma=2.05\pm 0.25$. These two values of γ differ by 2.7 standard deviations and indeed indicate that the angular correlations between like pions are influenced by the sharp peak in the forward direction [Fig. 1(c)]. It will not be possible, however, to obtain a quantitative answer as to the importance of the Bose effect[11] and/or π-π interaction without further extensive studies.

Reaction $\bar{p}+p\to 2\pi^-+2\pi^+$. On the basis of χ^2 and the missing mass, 136 4-prong events have been identified as Reaction (2). This is a 4-constraint case, and the maximum acceptable χ^2 was taken to be 36; about 65% of these events have $\chi^2<10$. The angular distribution of π^- (π^+) shows a forward (backward) peak [Fig. 1(d)].

Reaction $\bar{p}+p\to 2\pi^-+2\pi^++n\pi^0$. The remaining 810 events, which did not fit either Reaction (1) or (2), were assumed to be Reaction (3). However, this sample contains an estimated 16% of annihilations into K mesons, Reactions (4) to (7) (see below), in which K mesons have not decayed in the chamber. Because we transform our events into the c.m. system by ascribing pion mass to all charged prongs, the resultant c.m. angle will be wrong for these events. Also, this sample contains 4 prongs produced by π^- in the antiproton beam, whose contribution could be as high as 5%. In spite of this background, the angular distribution of π^- and π^+ exhibits features similar to the ones of Reactions (1) and (2) [Fig. 1(e)]. The average momentum is 369 ± 9 and 332 ± 5 Mev/c for forward and nonforward pions, respectively.

(ii) Reactions $\bar{p}+p\to\bar{K}+K+n\pi$. Of the 287 $K\bar{K}n\pi$ events, 135 were V-(2 prong) or V-(4 prong) events having a $K^+\bar{K}^0$ or K^-K^0 pair from the reactions

$$\bar{p}+p\to K^++\pi^-+\bar{K}^0+n_1\pi^0, \quad (4)$$

$$\bar{p}+p\to K^++\pi^++2\pi^-+\bar{K}^0+n_2\pi^0, \quad (5)$$

$$\bar{p}+p\to K^-+\pi^++K^0+n_3\pi^0, \quad (6)$$

and

$$\bar{p}+p\to K^-+\pi^-+2\pi^++K^0+n_4\pi^0. \quad (7)$$

As can be seen from the nature of Reactions (4) to (7), this sample contains a variety of types of events from the point of view of the fitting procedure, with the number of constraints 1, 3, and 4. Clearly each of these requires a separate set of criteria for identification. We shall give only a general outline: (a) The χ^2 distribution for each type of event agreed well with the expected distribution when it was divided by 3; (b) the missing mass distributions were used to determine the number of neutral particles (π^0's, or K^0 plus π^0's) associated with each event; and (c) the data were examined and found to be resaonably free of biases by looking at azimuthal distributions of events in the bubble chamber, their spatial distribution along the chamber, and the distribution of decay times for K^0 (or $\bar{K}^0$). The events were not generally ambiguous as to the number of missing neutral particles. For most of the events, only one

of the K mesons was observed to decay within the chamber. Some events are ambiguous as to which particle is the second K meson. The detailed procedure for the identification and disposition of the ambiguities of these events is given elsewhere.[12] The angular distribution of both K^- and π^- (K^+ and π^+) has exhibited a forward (backward) peak in a fashion similar to the ones of Reactions (1) to (3), as shown in the histograms in Figs. 2(a) and 2(b).

Our angular distribution indicates a possibility that two different annihilation mechanisms are operative: the statistical one, which is dominant and produces an isotropic angular distribution; and a dynamical mechanism responsible for the forward peak. Whereas the observed forward-to-backward ratio F/B is consistent with the model of Koba and Takeda,[13] it is not clear whether the fact that kaons show similar angular distribution features is consistent with that model, because it has never been extended in all its manifestations for the annihilations in flight.

The very recent data on antineutron-proton annihilations at our momentum indicate a possible excess of π^+ in the direction of the proton.[14]

It is a pleasure to acknowledge our particular indebtedness to L. W. Alvarez for his guidance and discussions, and to A. H. Rosenfeld for invaluable aid in the concept of the data analysis for this work. Thanks are due to J. Button, P. Eberhard, A. Hussain, J. Lanutti, G. Lynch, N. Xuong, C. Tate, and C. Rindfleisch for their help in various stages of the experiment.

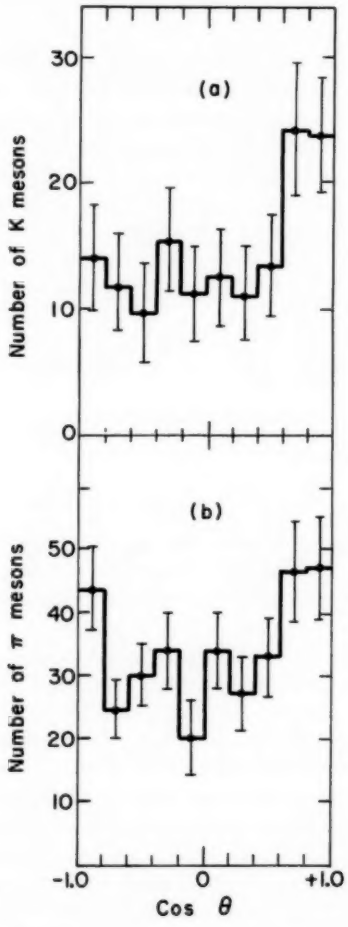

FIG. 2. Histograms of (a) combined angular distributions of K^- and reflected K^+ from Reactions (4) to (7); and (b) π^- and reflected π^+ from Reactions (4) to (7). The F/B ratio is 1.37 ± 0.18 and 1.24 ± 0.15 for distributions (a) and (b), respectively.

*This work was done under the auspices of the U. S. Atomic Energy Commission.

[1]E. Fermi, Progr. Theoret. Phys. (Kyoto) 5, 570 (1950). For review on annihilation see E. Segrè, Ann. Rev. Nuclear Sci. 8, 127 (1958). See also: P. Srivastava and G. Sudarshan, Phys. Rev. 110, 765 (1958); I. Pomeranchuk, Doklady Akad. Nauk S.S.S.R. 78, 889 (1951); F. Cerulus, Nuovo cimento 14, 827 (1959); S. Frautschi, Progr. Theoret. Phys. (Kyoto) 22, 15 (1959); B. Desai, Phys. Rev. 119, 1390 (1960); and G. Pinsky, G. Sudarshan, and K. Manhantappa, Proceedings of the 1960 International Conference on High-Energy Physics at Rochester (Interscience Publishers, Inc., New York, 1960), p. 173.

[2]Z. Koba and G. Takeda, Progr. Theoret. Phys. (Kyoto) 19, 269 (1958). This is mainly a model for annihilations at rest and does not discuss dynamic effects.

[3]G. Goldhaber, talk at CERN, November, 1960 (unpublished); also, S. Goldhaber, Bull. Am. Phys. Sec. 4, 417 (1959). See also reference 13.

[4]G. Lynch, J. Button, P. Eberhard, G. Kalbfleisch, J. Lannutti, B. Maglić, M. Stevenson, and N. Xuong, Bull. Am. Phys. Soc. 6, 40 (1961); also, G. R. Lynch, Revs. Modern Phys. 33, 395 (1961). The background problem is now being investigated, because these events also fit reaction $\bar{p}+p \rightarrow \pi^+ + \pi^- + \pi^0$.

[5]J. Button, P. Eberhard, G. Kalbfleisch, J. Lannutti, G. Lynch, B. Maglić, M. L. Stevenson, and N. H. Xuong, Phys. Rev. 121, 1788 (1961). Forward peaking is also observed in Λ emission from reaction $\bar{p}+p \rightarrow \bar{\Lambda}+\Lambda$.

[6]Reference Manual for KICK IBM Program, edited by A. H. Rosenfeld [Lawrence Radiation Laboratory Report UCRL-9099, 1961 (unpublished)]. See also A. H. Rosenfeld and J. N. Snyder, Lawrence Radiation Laboratory Report UCRL-9098, 1960 [Rev. Sci. Instr. (to be published)].

[7]A. Pais, Phys. Rev. Letters 3, 242 (1959).

[8]S. Z. Belenskij and L. D. Landau, Nuovo cimento 3, 15 (1956). For the predictions of other models see: S. Takagi, Progr. Theoret. Phys. (Kyoto) 7, 123 (1952); W. Heisenberg, Z. Physik 133, 65 (1952); H. Bhabha, Proc. Roy. Soc. (London) A219, 293 (1953); and G. Cocconi, Phys. Rev. 111, 1699 (1958). Charge distributions of the secondaries have not been considered in any of the ultrahigh-energy N-N interaction models.

[9]This is strictly true only when the number of pions emitted in an annihilation becomes infinite.

[10]G. Goldhaber, W. Fowler, S. Goldhaber, T. Hoang, T. Kalogeropoulos, and W. Powell, Phys. Rev. Letters 3, 181 (1959).

[11]G. Goldhaber, S. Goldhaber, W. Lee, and A. Pais, Phys. Rev. 120, 300 (1960).

[12]G. R. Kalbfleisch, Ph. D. thesis, Lawrence Radiation Laboratory Report UCRL-9597, 1961 (unpublished).

[13]Hartmut Pilkuhn, University of Stockholm (private communication).

[14]C. K. Hinrichs, Ph. D. thesis, Lawrence Radiation Laboratory Report UCRL-9589, 1961 (unpublished). Also, it has been communicated to us recently that the data at 1.05 Bev/c in propane (reference 11) tend to agree with our effect, with the ratio $F/B = 1.18 \pm 0.10$ [G. Goldhaber, University of California, Berkeley (private communication)].

SCATTERING OF Bev ELECTRONS BY HYDROGEN AND DEUTERIUM*

R. M. Littauer, H. F. Schopper,† and R. R. Wilson
Laboratory of Nuclear Studies, Cornell University, Ithaca, New York
(Received July 21, 1961)

At Cornell University, using the 1.3-Bev electron accelerator, measurements of the scattering of electrons by hydrogen and deuterium have been extended to new energies and angles. The cross section at 90° has been measured using the same equipment and procedure that were previously employed[1,2] at 66° and 112°. A new quadrupole magnet spectrometer of large solid angle has been placed at 45° or at 135° so that measurements could be made at two angles simultaneously. In Table I are shown the new results at 45°, 90°, and 135°, while all of the Cornell measurements are summarized in Fig. 1.

The hydrogen cross section, $d\sigma/d\Omega$, was determined in a straightforward manner. We have used the Schwinger correction for radiation. For the deuteron, the differential cross section $d^2\sigma/dE'd\Omega$ was measured at the energy where the electrons scattered from protons give an elastic peak. Then the total deuteron cross section, shown in Fig. 1, was calculated from this deuteron peak cross section using the impulse approximation as given by Goldberg.[3] Most recently, Durand[4] derived Goldberg's formula more rigorously and showed that it is accurate to within a few percent.

Table I. Differential cross sections for elastic scattering of electrons of energy E_0 by protons, and peak cross sections for scattering by deuterons. All parameters in the laboratory frame. Schwinger correction applied.

E_0 (Mev)	Proton $(d\sigma/d\Omega)\times10^{32}$ (cm^2/sr) 45°	90°	135°	Deuteron $(d^2\sigma/dE'd\Omega)\times10^{33}$ (cm^2/Mev sr) 45°	90°	135°
317		6.04 ±0.24	1.21 ±0.08		2.14 ±0.14	0.623 ±0.080
387	92.5 ±4.0	3.61 ±0.15	0.790 ±0.031	31.2 ±2.0	1.29 ±0.05	0.307 ±0.026
407	81.0 ±1.9			31.2 ±0.7		
465		1.91 ±0.06	0.296 ±0.019		0.635 ±0.04	0.130 ±0.011
552	37.5 ±1.1			10.9 ±0.3		
565		0.815 ±0.08	···		0.330 ±0.03	···
600		0.99 ±0.03	0.178 ±0.008		0.333 ±0.015	0.0638 ±0.004
664	22.0 ±0.7			5.88 ±0.3		
720		0.388 ±0.017	0.0732 ±0.005		0.132 ±0.010	0.0248 ±0.0032
800	10.4 ±0.5			2.68 ±0.15		
836		0.212 ±0.01	0.0302 ±0.005		0.0448 ±0.003	0.0121 ±0.0026
941	6.63 ±0.3			1.39 ±0.06		
974		0.080 ±0.014	0.0272 ±0.004		0.0147 ±0.003	0.0083 ±0.0024
1050	4.68 ±0.2			0.76 ±0.04		
1136		0.0362 ±0.0028	0.0117 ±0.004		0.0107 ±0.003	0.0033 ±0.0015
1166	3.24 ±0.17			0.61 ±0.06		

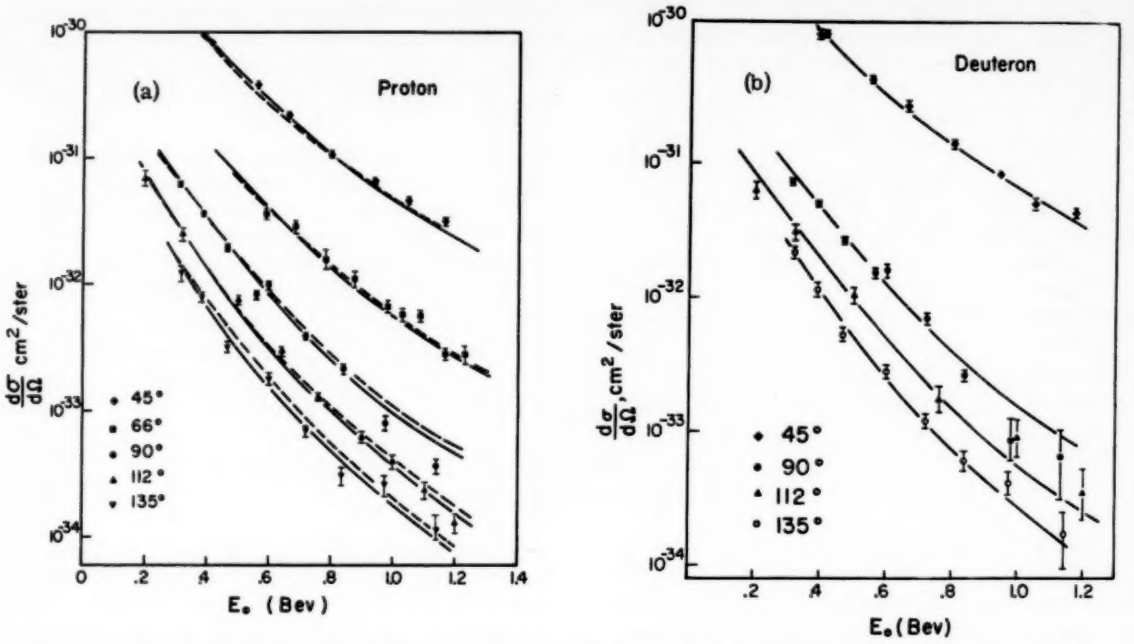

FIG. 1. Differential elastic scattering cross section for the proton (a) and the deuteron (b), as a function of incident electron energy and laboratory scattering angle. Full curves computed with core model, dashed curves according to Bergia et al. See R. M. Littauer et al., following Letter [Phys. Rev. Letters 7, 144 (1961)].

Figure 2 illustrates the determination of the electric form factors F_1 and the magnetic form factors F_2 by the intersecting ellipse method.[5] For a given value of q^2, the square of the momentum-energy transfer, one ellipse in the F_1-F_2 plane is determined by a measurement of the cross section at a par-

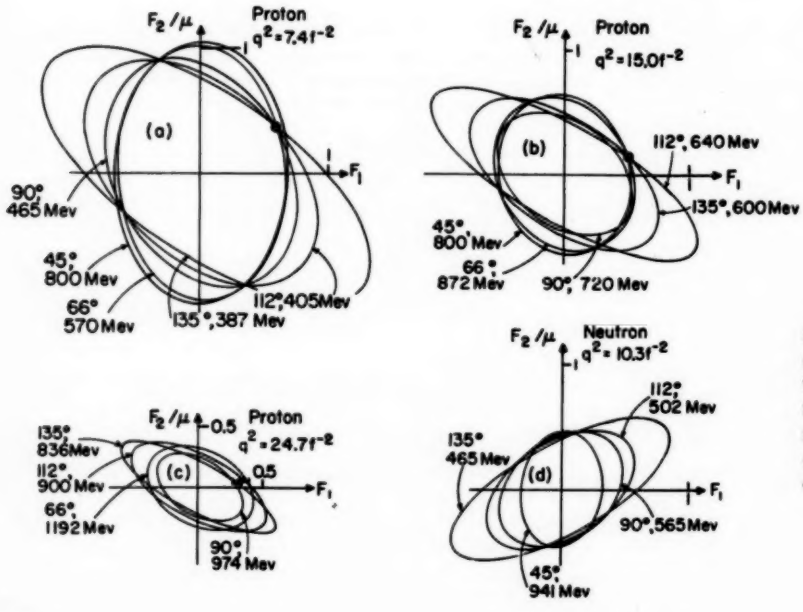

FIG. 2. Determination of F_1 and F_2 by the method of intersecting ellipses. Examples for the proton at q^2=7.4 f^{-2} (a), 15.0 f^{-2} (b), and 24.7 f^{-2} (c); for the neutron at q^2=10.3 f^{-2} (d). In each case the abscissa is F_1, the ordinate F_2/μ.

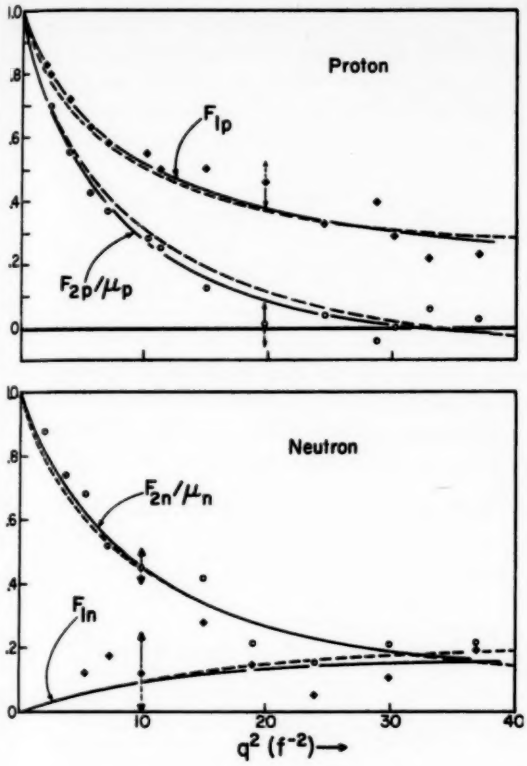

FIG. 3. Electric and magnetic form factors for the proton and neutron. The points are obtained by the intersecting-ellipse method; thus, errors for F_1 and F_2 are not independent. Typical acceptable deviations are indicated, in correlated senses, by the solid and broken arrows. The solid curve shows a fit to the data by the core model, the dashed curve by the Clementel-Villi form.

ticular angle. Other measurements at different angles but at the same q^2 determine other ellipses. (The form factors are presumed to be functions of q^2 only.) The intersections[6] give specific values of F_1 and F_2 which have been plotted against q^2 in Fig. 3.

In our previous measurements of the scattering from deuterium we had results at but one angle; hence, in analyzing our data we necessarily made the assumption that $F_{2n} = -F_{2p}$. This assumption, of course, is now no longer made in finding the results shown in Fig. 3; we find, in agreement with the recent Stanford measurements,[7] that $-F_{2n}$ becomes larger than F_{2p} especially at high values of q^2, where F_{2p} is small or might even go negative while $-F_{2n}$ is still positive. These new values of F_{2n} do not seriously change our previously deduced values of F_{1p} (by less than the statistical error), but they do indicate that it is necessary to assign a small negative magnetic moment to the core of the proton and neutron which gives rise to a small isoscalar part of the magnetic form factors.

Our values of F_{1n}/μ_n are positive and between 0.1 and 0.2, in agreement with the earlier Stanford results[7] calculated with a modified Jankus theory.[8,5] This disagrees, however, with the reinterpretation of the Stanford results by Durand,[4] which yields values of F_{1n}/μ_n that are small or may even go negative.

---

*Supported in part by joint contract of Office of Naval Research and the U. S. Atomic Energy Commission.

†On leave from the Technische Hochschule Karlsruhe, Germany.

[1]R. Wilson, K. Berkelman, J. Cassels, and D. Olson, Nature 188, 94 (1960).

[2]D. N. Olson, H. F. Schopper, and R. R. Wilson, Phys. Rev. Letters 6, 286 (1961).

[3]A. Goldberg, Phys. Rev. 112, 618 (1958).

[4]L. Durand, III, Phys. Rev. Letters 6, 631 (1961); and to be published.

[5]R. Herman and R. Hofstadter, High-Energy Electron Scattering Tables (Stanford University Press, Stanford, California, 1960).

[6]It can be shown that if there were no experimental errors all ellipses for a certain q value would intersect in the same four points. The question is which intersection gives the right values for F_1 and F_2. Two of these intersections are reflections of the other two in the origin and can be eliminated since they imply only a trivially different normalization. The choice between the remaining two intersections cannot be made on the basis of the experimental results alone. However, it is evident that F_{1p} has to be positive since F_{1p} approaches +1 for $q \to 0$. Furthermore, one expects that the charge in the proton and neutron core has the same sign, which implies that F_{1n} has the same sign as F_{1p}, i.e., positive.

[7]R. Hofstadter and R. Herman, Phys. Rev. Letters 6, 293 (1961).

[8]V. Z. Jankus, Phys. Rev. 102, 1589 (1956).

STRUCTURE OF THE PROTON AND NEUTRON*

R. M. Littauer, H. F. Schopper,† and R. R. Wilson
Laboratory of Nuclear Studies, Cornell University, Ithaca, New York
(Received July 3, 1961; revised manuscript received July 21, 1961)

We have previously analyzed our data[1] to show that the proton and neutron have a common core of positive charge of about $0.35e$, whose radius might be about 0.2 fermi. This core is surrounded by a meson cloud of radius 0.8 f, with an average charge which changes from $+0.5e$ for the proton to $-0.5e$ for the neutron. Additionally, we found it necessary to postulate another cloud, the same for the neutron and proton, with a positive charge of $0.15e$ and an rms radius of about 1.4 f, thus extending out beyond the meson cloud. These clouds of charge take on meaning in the simple A model of the nucleon put forward by Bergia, Stanghellini, Fubini, and Villi,[2] referred to herein as BSFV. Their model is based on dispersion theory and on a two-pion interaction similar to that used by Frazer and Fulco.[3] In this model they identify the meson cloud with a $T=1$, $J=1$ two-pion resonant state while the extended cloud might correspond to a three-meson resonant state, most probably with $T=0$ and $J=1$. Our new measurements,[4] when examined in the light of the above model of the nucleon, imply that the resonant energy of the two-pion state is $4.0m_\pi$ and that of the three-pion state is $2.9m_\pi$.

Let us now analyze our form factors into isoscalar and isovector partial form factors[5]:

$$F_{1p}=F_{1S}+F_{1V};\quad F_{1n}=F_{1S}-F_{1V},$$
$$F_{2p}=F_{2S}+F_{2V};\quad F_{2n}=F_{2S}-F_{2V}. \tag{1}$$

In making our simple core model analysis, we got a vanishing rms radius for the neutron charge distribution by resolving the isoscalar form factor F_{1S} of Eq. (1) further into two terms, i.e., $F_{1S}=F_{1S}^{\text{core}}+F_{1S}^{\text{cl}}$, where we associated F_{1S}^{core}, the term with the smaller radius, with the core of the nucleon, and F_{1S}^{cl}, with an extended cloud. Our new results can best be fitted by partial form factors corresponding to exponential density distributions. Partial form factors of Gaussian or other shape without a singularity give a worse fit. We write therefore

$$F_{1S}=e_s^{\text{core}}(1+a_{s,\text{core}}^2q^2/12)^{-2}+e_s^{\text{cl}}(1+a_{s,\text{cl}}^2q^2/12)^{-2},$$
$$F_{1V}=e_v(1+a_v^2q^2/12)^{-2}, \tag{2}$$

where the a's are the rms radii of the respective charge distributions. In order to obtain the right total charges and rms radii for the proton and neutron, the following conditions must hold:

$$e_s^{\text{core}}+e_s^{\text{cl}}+e_v=1,$$
$$e_s^{\text{core}}+e_s^{\text{cl}}-e_v=0,$$
$$e_s^{\text{core}}a_{s,\text{core}}^2+e_s^{\text{cl}}a_{s,\text{cl}}^2+e_va_v^2=a_p^2,$$
$$e_s^{\text{core}}a_{s,\text{core}}^2+e_s^{\text{cl}}a_{s,\text{cl}}^2-e_va_v^2=a_n^2. \tag{3}$$

Assuming that $a_{s,\text{core}}^2\ll a_{s,\text{cl}}^2$ and because $a_n^2=0$, one obtains

$$e_v=\tfrac{1}{2},\quad e_s^{\text{core}}+e_s^{\text{cl}}=\tfrac{1}{2},$$
$$a_v^2=2e_s^{\text{cl}}a_{s,\text{cl}}^2=a_p^2. \tag{4}$$

These conditions restrict the six adjustable parameters so that only two are left to fit the experimental data at higher q values, e.g., e_s^{core} and $a_{s,\text{core}}$.

To describe our newly determined magnetic form factors, we now assign partial magnetic moments μ_s^{core}, μ_s^{cl}, μ_v to the same core and clouds that we have used to describe the charge distributions and we write

$$F_{2S}=\mu_s^{\text{core}}(1+b_{s,\text{core}}^2q^2/12)^{-2}+\mu_s^{\text{cl}}(1+b_{s,\text{cl}}^2q^2/12)^{-2},$$
$$F_{2V}=\mu_v(1+b_v^2q^2/12)^{-2}, \tag{5}$$

where $b_{s,\mathrm{core}}$, $b_{s,\mathrm{cl}}$, and b_v are the rms radii of the partial form factors for the magnetic moment and all magnetic moments are measured in nuclear magnetons (nm).

In exactly the same manner as for the partial electric charges, we can infer the conditions

$$\mu_s^{\mathrm{core}} + \mu_s^{\mathrm{cl}} + \mu_v = \mu_p = 1.793 \text{ nm},$$

$$\mu_s^{\mathrm{core}} + \mu_s^{\mathrm{cl}} - \mu_v = \mu_n = -1.913 \text{ nm},$$

$$\mu_s^{\mathrm{core}} b_{s,\mathrm{core}}^2 + \mu_s^{\mathrm{cl}} b_{s,\mathrm{cl}}^2 + \mu_v b_v^2 = \mu_p b_p^2,$$

$$\mu_s^{\mathrm{core}} b_{s,\mathrm{core}}^2 + \mu_s^{\mathrm{cl}} b_{s,\mathrm{cl}}^2 - \mu_v b_v^2 = \mu_n b_n^2. \quad (6)$$

From these one readily obtains with $b_{s,\mathrm{core}}^2 \ll b_{s,\mathrm{cl}}^2$:

$$\mu_v = 1,$$

$$\mu_s^{\mathrm{core}} + \mu_s^{\mathrm{cl}} = (\mu_p + \mu_n)/2 = -0.060 \text{ nm}, \quad (7)$$

$$2\mu_s^{\mathrm{cl}} b_{s,\mathrm{cl}}^2 = \mu_p b_p^2 + \mu_n b_n^2,$$

$$2\mu_v b_v^2 = \mu_p b_p^2 - \mu_n b_n^2. \quad (8)$$

A consequence of these conditions is again that only two parameters, e.g., μ_s^{core} and $b_{s,\mathrm{core}}$, are left to fit the data at high q values, if b_p^2 and b_n^2 are obtained from the slope of the form factors at small q values.

Table I. Best-fit parameters for core model with exponential density distributions. See text for definition of symbols.

e_s^{core}	= 0.25	$a_{s,\mathrm{core}}$	= 0.2 f
e_s^{cl}	= 0.25	$a_{s,\mathrm{cl}}$	= 1.13 f
e_v	= 0.5	a_v	= 0.80 f
μ_s^{core}	= -0.22	$b_{s,\mathrm{core}}$	undetermined
μ_s^{cl}	= 0.16	$b_{s,\mathrm{cl}}$	= 1.30 f
μ_v	= 1.853	b_v	= 0.89 f
a_p	= 0.80 f	b_p	= 0.98 f
a_n	= 0	b_n	= 0.79 f

At large values of q^2, the effect of the extensive isoscalar cloud will be negligible and we can fit the core parameters. A point moment of -0.19 nm would give a satisfactory fit, but let us ascribe to the core, arbitrarily, the same rms radius of 0.2 f which fits the charge core. In this case, the core moment must be -0.22 nm. In order to make the static moments correct, we must then ascribe a magnetic moment of +0.16 nm to the extended isoscalar cloud so that the total isoscalar moment $= \frac{1}{2}(\mu_p + \mu_n) = -0.060$ nm, as required by (7).

Table I summarizes the parameters we have found for the partial form factors; these are plotted in Fig. 1, and the corresponding spatial distributions are shown in Fig. 2.

The qualitative result then of these new measurements is that we find it necessary to attribute a magnetic moment of negative sign to the charge core that our previous measurement had revealed. It is not unreasonable that the angular momentum of the meson cloud be unity; then necessarily the core will have a spin of $-\frac{1}{2}$, which might rather

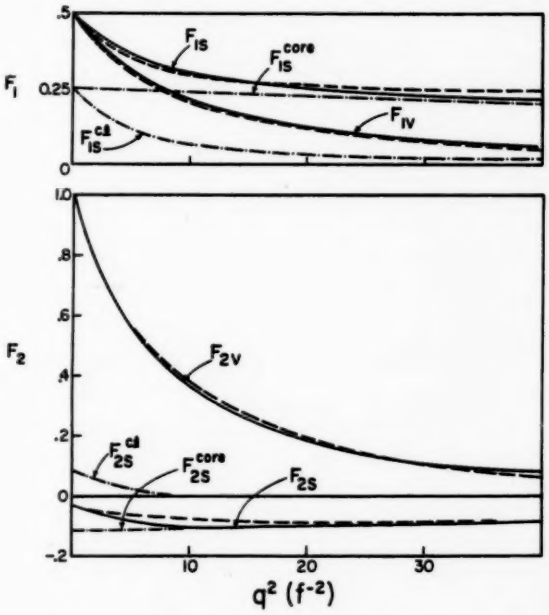

FIG. 1. Partial form factors for F_1 and F_2. Each form factor is resolved into isoscalar and isovector parts, whose sum and difference give, respectively, the neutron and proton form factors. The solid curves indicate the fit according to the core model, where the scalar partial form factors have been further split into terms corresponding to a core and an extended cloud, each of exponential distribution. The dashed curves indicate the best fit obtained by the Clementel-Villi form.

naturally give rise to the negative magnetic moment—for example, by dissolution of the core into a $K^+\Lambda$ system in direct analogy to pion emission. It is also perhaps significant that the radius of the extended isoscalar cloud of magnetic moment comes out so close to that of the isoscalar charge cloud—also true of the isovector clouds.

BSFV have proposed aesthetically simple form factors for the nucleon based on the model already referred to above. In our notation their form factors are

$$F_2^{\,v}=\tfrac{1}{2}\left[(1-\alpha_v)+\frac{\alpha_v}{1+q^2/q_v^{\,2}}\right],\quad F_2^{\,v}=1.853\left[(1-\beta_v)+\frac{\beta_v}{1+q^2/q_v^{\,2}}\right],\tag{9}$$

$$F_1^{\,s}=\tfrac{1}{2}\left[(1-\alpha_s)+\frac{\alpha_s}{1+q^2/q_s^{\,2}}\right],\quad F_2^{\,s}=-0.060\left[(1-\beta_s)+\frac{\beta_s}{1+q^2/q_s^{\,2}}\right],\tag{10}$$

where one minus the constants α or β give the fraction of the charge or magnetic moment in a point core, and α_s or α_v give the corresponding fraction in a Yukawa meson cloud of mean square radius $6/q_s^{\,2}$ or $6/q_v^{\,2}$. It appears that BSFV have, not unreasonably, assumed that the radii of the Yukawa clouds that appear in F_1 and F_2 are the same. They show that the radius of the Yukawa part of the isovector partial form factor is due to a $T=1$, $J=1$ two-pion resonant state with the resonance at q_v, while the isoscalar radius will correspond to a three-meson resonant state, most probably with $T=0$, $J=1$, at q_s. The six parameters in (9) and (10) are reduced to five because the experimental requirement that the neutron charge radius is zero leads to the relation

$$a_s/q_s^{\,2}=a_v/q_v^{\,2}.\tag{11}$$

Table II gives values of the five independent parameters that best fit our data plus the rms radii of the neutron and proton. The same parameters have also been determined at Stanford[6] and their values in our nomenclature are shown for com-

Table II. Parameters for best fit according to BSFV[a] form.

	Cornell	Stanford
α_v	1.10	1.20
β_v	1.14	1.20
α_s	0.58	0.56
β_s	-1.5	-3.0
a_v	0.85 f	0.77 f
a_s	1.16 f	1.13 f
a_p	0.88 f	0.85 f
b_p	0.95 f	0.94 f
b_n	0.87 f	0.76 f
$q_v^{\,2}$	$8.3\ \mathrm{f}^{-2}=16(m_\pi/c)^2$	$10\ \mathrm{f}^{-2}=19.6(m_\pi/c)^2$
$q_s^{\,2}$	$4.4\ \mathrm{f}^{-2}=8.5(m_\pi/c)^2$	$4.7\ \mathrm{f}^{-2}=9(m_\pi/c)^2$

[a]See reference 2.

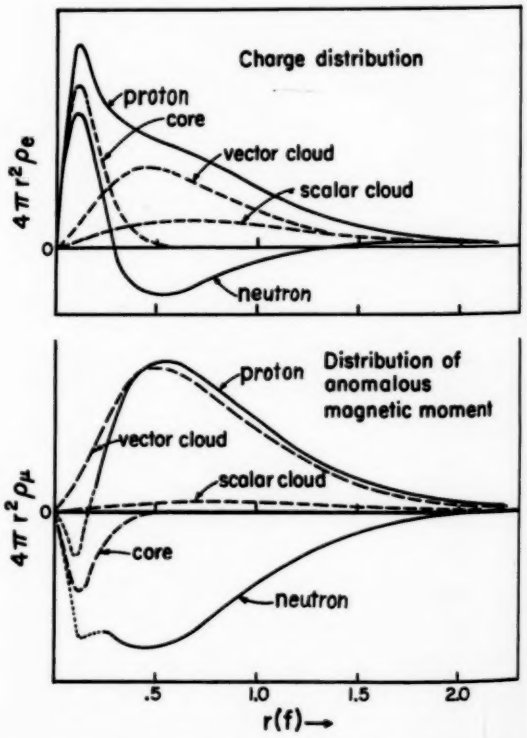

FIG. 2. Spatial distribution of charge and anomalous magnetic moment for proton and neutron, according to the core model.

parison; the general agreement is good. Slight discrepancies arise mainly because our experimental values for F_{2p} at high q^2 values are close to zero whereas an extrapolation of the Stanford form factors gives negative values. Our experiments indicate also a somewhat smaller difference between F_{2p} and F_{2n}.

The experimental data are fit equally well by the BSFV form factors or by those following from our simple core model (see Fig. 1 and the curves in the preceding Letter[4]).

According to the interpretation of BSFV, our values of q_v and q_s would imply that the resonant energy of the two-pion state is $4.0\,m_\pi$ and that of the three-pion state is $2.9\,m_\pi$.

*Supported in part by joint contract of Office of Naval Research and the U. S. Atomic Energy Commission.

†On leave from the Technische Hochschule Karlsruhe, Germany.

[1]D. N. Olson, H. F. Schopper, and R. R. Wilson, Phys. Rev. Letters 6, 286 (1961).

[2]S. Bergia, A. Stanghellini, S. Fubini, and C. Villi, Phys. Rev. Letters 6, 367 (1961).

[3]W. Frazer and J. Fulco, Phys. Rev. 117, 1609 (1960).

[4]R. M. Littauer, H. F. Schopper, and R. R. Wilson, preceding Letter [Phys. Rev. Letters 7, 141 (1961)].

[5]Our normalization, following BSFV, is such that the value of the form factor at $q^2=0$ gives either the static charge or magnetic moment as the case may be. Thus F_1 normalizes to unity or zero for the proton or neutron, and F_2 normalizes to the appropriate anomalous magnetic moment measured in nuclear magnetons. The Rosenbluth scattering formula then must be written in the form

$$\frac{d\sigma}{d\Omega}=\sigma_0\left\{F_1^2+\frac{q^2}{4M^2}\left[2(F_1+F_2)^2\tan^2(\theta/2)+F_2^2\right]\right\},$$

i.e., the different proton and neutron cross sections result directly from inserting the different values of F_1 and F_2 that are given by (1). We can speak of a partial charge or a partial magnetic moment whose value is given by the value of the corresponding partial form factor at $q^2=0$, the total charge or moment being the sum of the partial charges or partial moments.

[6]R. Hofstadter and R. Herman, Phys. Rev. Letters 6, 293 (1961); see, however, the reinterpretation of some of these results by L. Durand, III, Phys. Rev. Letters 6, 631 (1961).

X-RAY YIELDS IN THE K AND L SERIES OF μ-MESONIC ATOMS*

J. L. Lathrop, R. A. Lundy, V. L. Telegdi, and R. Winston
The Enrico Fermi Institute for Nuclear Studies, The University of Chicago, Chicago, Illinois
(Received July 14, 1961)

Since the experimental work of Stearns and Stearns,[1] much theoretical speculation has been presented[2-7] to account for the low yields of x-rays in the K and L series of light μ-mesonic atoms reported by these authors. Their results, reproduced in Figs. 1(a) and 1(b) (filled circles), require that the Auger rates[8] competing with radiative transitions be, respectively, ~300 times (K series) or ~30 times (L series) as fast as predicted by conventional theory, or else that one postulate some hithertofore unknown competitive transition mechanism. The situation for the yields of π-mesonic x rays of comparable energies is entirely similar,[9] but need not be discussed here.

In view of this situation, we decided to remeasure the yields in the π-mesonic K and L series, in particular for those light elements for which low (or even experimentally unobservable) yields were reported in reference 1. In view of our findings, we think it useful to present here our preliminary results. They are displayed in Figs. 1(a) and 1(b) (open circles).

The experimental arrangement used by us is shown in Fig. 2 and is essentially the same as that used by Stearns and Stearns.[1] Some relevant differences are the following: (a) use of thinner (1/16 in.) plastic scintillators, wrapped in 1-mil Al foil, just before and just behind the x ray target T, to improve the transmission of soft x rays and to decrease the background of carbon mesonic x rays; (b) use of an improved window (20 mils of Be) on the 1/16-in., 2-in.-diameter NaI detector employed for x rays up to 75 kev; (c) use of a longer effective resolving time (100 nsec vs the 50 nsec of Stearns and Stearns) for NaI-induced coincidences; (d) use of a 100-channel pulse-height analyzer (RIDL 34).

The running conditions differed more markedly from those available to earlier workers in this field, in the following respects: (a) use of a μ^- beam of low e^- content and of a Čerenkov counter (No. 3 in Fig. 2) for further electron rejection; (b) use of a good duty-cycle (~5) meson beam, obtained by means of a vibrating cyclotron target.[10] These conditions enabled us to use rather slow NaI coincidences without generating large accidental backgrounds. As is well known, hard clipping of NaI pulses of small amplitude (from, say,

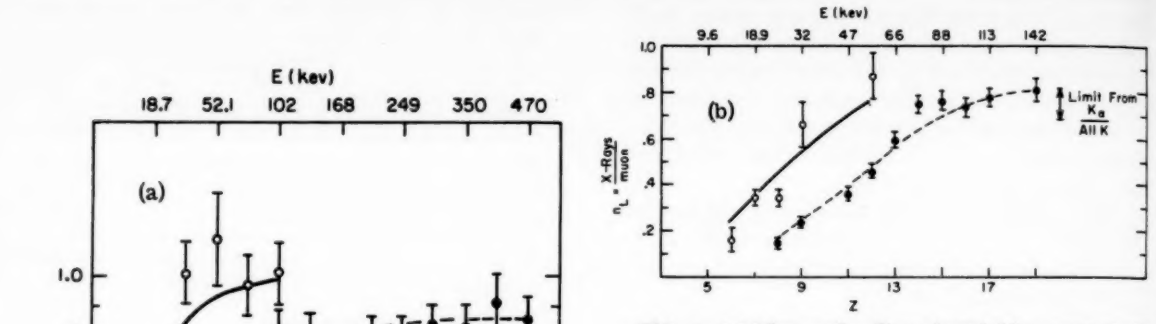

FIG. 1. (a) Observed μ K-series yields: open circles, this experiment; filled circles, reference 1. Curves are fits to $n_K = \text{const}\ Z^4/(Z^4+C_1)$. For this experiment, const = 1.00, $C_1 = 45$, while const = 0.86, $C_1 = 450$ for reference 1. With the same assumptions as used in reference 1, present data require an Auger transition probability about 30 × theoretical. Note that the sole evidence for fall of K yield with low Z rests on the Li K point. (b) Observed μ L-series yields: open circles, this experiment; filled circles, reference 1. Curves are fits to $n_L = \text{const}\ Z^4/(Z^4+C_2)$. For this experiment, const = 0.80, $C_2 = 3\times10^3$, while const = 0.97, $C_2 = 2\times10^4$ for reference 1. With the same assumptions as used in reference 1, present data require an Auger transition probability about 4 × theoretical.

25-kev photons) can easily lead to large time jitters and hence appreciable coincidence losses. The limiter (see Fig. 2) used by us was well cut off by 12-kev x rays from a Hg^{203} source under the operating conditions of the NaI detector; further, during actual runs a good plateau (< 2% slope/100 v at 2100 v photomultiplier voltage) was obtained with Li K x rays (19 kev).

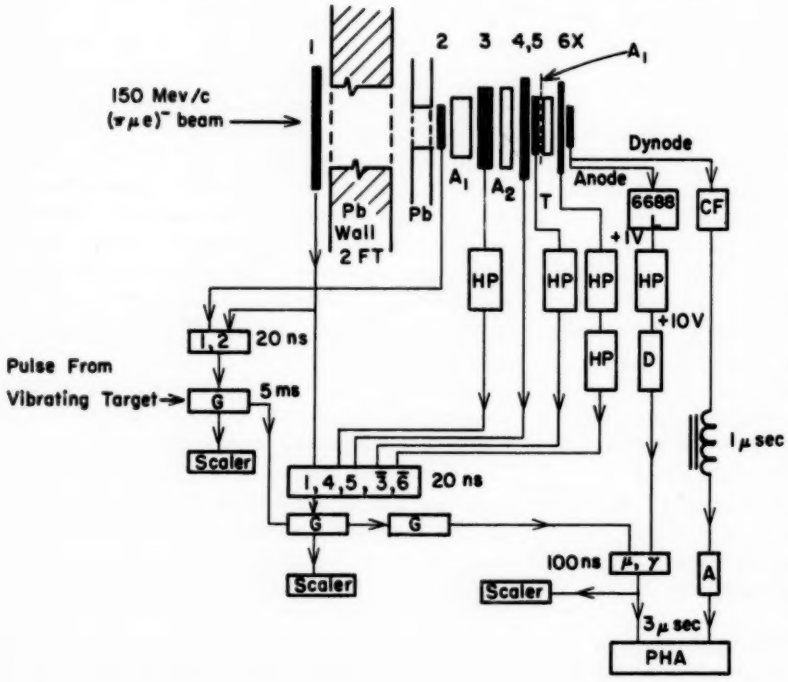

FIG. 2. Experimental arrangement: 1, 2, 4, 5, and 6 are plastic scintillators, viz., 1 = 6 × 6 × 3/8 in., 2 = 3 × 3 × 1/4 in., 4 = 5 × 5 × 1/8 in., 5 = 3 × 3 × 1/16 in., 6 = 4.5 × 4.5 × 1/16 in., 4 = 4 × 4 × 1 in. H_2O − Cerenkov counter, X = 2-in.-diam × 1/16-in. NaI crystal, connected by logarithmic light pipe to a 5-in.-diameter photomultiplier (10-stage EMI). A_1, A_2, A_3 absorbers; A_1 = 2 in. graphite, A_2 = 0.75 in. Cu, A_3 = 0.008 in. brass (shield for x rays from counter 5); T, target (in Table I; L = limiter; CF = cathode follower; HP = distributed amplifier, gain 10; D = fast discriminator; G = 5-msec gates; A = linear amplifier; PHA = 100-channel analyzer. (1,2), (1453$\bar{6}$), and ($\mu\gamma$) are coincidence circuits with the indicated resolutions.

Table I. Experimental data used for yield evaluation.

Element	Target thickness (g/cm^2)	Series, K_α (L_α) (kev)	Stopped[b] Muons $\times 10^3$ (corrected)	Calibration source	Counting[c] efficiency correction	Detected[d] x rays	K_α all K (%)	Series yield[e] Muon
Li	Metal, 1.2	K, 18.7	35.1	18 kev, Am^{241}	0.091	1.700	0.70	0.53 ± 0.05
Be	Metal, 1.5	K, 33.3	76.3	32 kev, Cs^{137}	0.078	6.061	0.82	1.01 ± 0.10
C	Graphite, 1.2	K, 75.0	18.9	73 kev, Hg^{203}	0.086	1.592	0.71	0.97 ± 0.10
C	Graphite, 0.48	L, 13.9	44.6	12 kev, Hg^{203}	0.067	0.475	0.63	0.16 ± 0.05
B	Powder, 1.9[a]	K, 52.1	52.0	52 kev, Tm^{170}	0.093	5.475	0.77	1.12 ± 0.17
N	95% $(NH_2)_n$	K, 102	29.9	60 kev, Am^{241}	0.16	4.836	0.69	1.01 ± 0.10
	+5% H_2O, 1.0[a]	L, 18.9	34.6	18 kev, Am^{241}	0.077	0.889	0.63	0.34 ± 0.03
O	Ice, 1.0	L, 25	32.7	32 kev, Cs^{137}	0.088	0.964	0.68	0.32 ± 0.03
F	LiF, 1.0[a]	L, 32	23.2	32 kev, Cs^{137}	0.087	1.334	0.81	0.66 ± 0.10
Mg	Metal, 2.0	L, 56	36.6	60 kev, Am^{241}	0.091	2.892	0.75	0.87 ± 0.04

[a] Contained in 3-inch diameter × 1/16-inch wall bakelite cylinder with 0.02-inch Lucite end windows.

[b] Fraction of muon stops in other than target material was measured.

[c] Includes empirically determined target, ac counter, and NaI casing attenuation, in- and out-scattering, and NaI efficiency (escape correction theoretical for Be K).

[d] All runs with 2-inch diameter × 1/16-inch NaI detector except N K with 3-inch diameter × 1/4-inch NaI detector; C K background was measured independently, C L background from counter No. 5 was filtered out with 0.008 inch brass.

[e] Indicated errors are increased over statistical to include error in analyzing spectra for background and error in absolute calibration with sources.

Table I summarizes the experimental data leading to the yields plotted in Figs. 1(a) and 1(b). The targets were in general 3-in. diameter cylinders, matched in surface density for roughly equal attenuation (~10%) of the mesonic x rays under study, rather than for equal stopping power,[1] and subtending approximately equal solid angles at the detector; the number of stopped particles was determined experimentally. The targets were calibrated in situ with uniform extended radioactive sources of calibrated intensity[11] yielding photons of energies close to those of the mesonic x rays of interest. Further calibrations, mainly for in- and out-scattering, were performed in the laboratory by displacing extended sources through appropriately subdivided targets. The important escape correction (~35%) for the Be K radiation (33 kev) had to be taken from theory[12] because no radioactive sources yielding photons as close to the iodine K edge (33.2 kev) were available. Dead-time corrections to the data stored in the pulse-height analyzer were negligible (10 analyses/sec, 100-μsec analysis time).

As is evident from Figs. 1(a) and 1(b), our results do not appear to bear out those of reference 1. Assuming that the mesons have a statistical distribution of $2l+1$ in the $n=14$ level, their results require an Auger rate of 5.85×10^{13} sec^{-1} (~300× "theoretical") for the K series and an Auger rate of 2.68×10^{14} sec^{-1} (~30×"theoretical") for the L series. In both cases the remaining "discrepancy" is an order of magnitude less serious than suggested by reference 1. By making different, but not unreasonable assumptions about the initial populations,[13] one can hope to reduce the extant "discrepancy" even further.

It has occasionally been suggested that the results of Stearns and Stearns[1] could be attributed to a thin "dead layer" on the front face of their NaI(Tl) crystal, or of such crystals in general. This hypothesis is not only at variance with general experience with NaI(Tl) detectors, but also fails to provide a satisfactory explanation. The effect of such a "dead layer" should be quite different for x ray energies just below, and just above, the iodine K edge, i.e., for Be K_α (33.3 kev) and F L_α (32 kev). The yields of reference 1 show no great variation between these two x rays.

Another suggestion frequently advanced is that the muon may be "trapped" in some high-n orbit. We briefly investigated this possibility by delaying the μ input to the μ-γ coincidence circut (see Fig. 2) by 100 nsec and looking for Li K x rays, the ones for which we find the lowest K yield. Not more than (1.0 ± 0.5)% "delayed" x rays were found in this way. This observation is most naturally interpreted in terms of some residual jit-

ter of the NaI pulse, but can clearly not preclude the existence of a long-lived delayed component. In the case of the π^- mesons, recent work at CERN[13] suggests, however, negligible trapping in Be.

A repetition of the present μ-mesonic yield measurements with a proportional counter is in progress, and an extension to pions is contemplated.

---

*Research supported by a joint program of the Office of Naval Research and the U. S. Atomic Energy Commission.

[1]M. B. Stearns and M. Stearns, Phys. Rev. 105, 1573 (1957).

[2]T. B. Day and P. Morrison, Phys. Rev. 107, 912 (1957).

[3]J. Bernstein and T. Y. Wu, Phys. Rev. Letters 2, 404 (1959).

[4]N. A. Krall and E. Gerjuoy, Phys. Rev. Letters 3, 142 (1959).

[5]M. A. Ruderman, Phys. Rev. 118, 1632 (1960).

[6]R. A. Ferrell, Phys. Rev. Letters 4, 425 (1960).

[7]Y. Eisenberg and D. Kessler, Nuovo cimento 6, 1195 (1961).

[8]G. R. Burbidge and A. H. de Borde, Phys. Rev. 89, 189 (1953); A. H. de Borde, Proc. Phys. Soc. (London) A67, 57 (1954).

[9]M. Stearns and M. B. Stearns, Phys. Rev. 107, 1709 (1957); M. Stearns, M. B. Stearns, and L. Leipuner, Phys. Rev. 108, 445 (1957); M. Camac, M. L. Halbert, and J. B. Platt, Phys. Rev. 99, 905 (1955).

[10]J. Rosen, Bull. Am. Phys. Soc. 6, 9 (1961); J. Rosen, Nevis Report No. 92 (unpublished).

[11]We are greatly indebted to Dr. D. W. Engelkemeir of Argonne National Laboratory for providing us with calibrated sources.

[12]T. B. Novey, Phys. Rev. 89, 672 (1953), Eq. (3). A slight correction to this formula must be made, the fluorescence yield of iodine being about 0.80 and not unity.

[13]R. A. Mann and M. E. Rose, Phys. Rev. 121, 293 (1961).

[14]G. Culligan, D. Harting, L. Madansky, and G. Tibell (to be published).